Environment International 194 (2024) 109151

Contents lists available at ScienceDirect

Environment International

journal homepage: www.elsevier.com/locate/envint

Full length article

Exploring environmental modifiers of LRRK2-associated Parkinson's disease penetrance: An exposomics and metagenomics pilot study on household dust

Begoña Talavera Andújar [a,*], Sandro L. Pereira [a], Susheel Bhanu Busi [a,b], Tatiana Usnich [c], Max Borsche [c,d], Sibel Ertan [e], Peter Bauer [f], Arndt Rolfs [f], Soraya Hezzaz [a], Jenny Ghelfi [a], Norbert Brüggemann [c,d], Paul Antony [a], Paul Wilmes [a,g,1], Christine Klein [c,1], Anne Grünewald [a,1], Emma L. Schymanski [a,1,*]

[a] Luxembourg Centre for Systems Biomedicine (LCSB), University of Luxembourg, L-4367 Belvaux, Luxembourg
[b] UK Centre for Ecology and Hydrology, Wallingford, Oxfordshire, United Kingdom
[c] Institute of Neurogenetics, University of Lübeck, Lübeck, Germany
[d] Department of Neurology, University of Lübeck, Lübeck, Germany
[e] School of Medicine, Department of Neurology, Koc University, Istanbul, Turkey
[f] CENTOGENE GmbH, Rostock, Germany
[g] Department of Life Sciences and Medicine, Faculty of Science, Technology and Medicine, University of Luxembourg, L-4362 Esch-sur-Alzette, Luxembourg

ARTICLE INFO

Handling Editor: Olga Kalantzi

Keywords:
Indoor environment
Exposomics
Metagenomics
Parkinson's disease
Leucine-rich repeat kinase 2 (LRRK2)
Bisphenol S

ABSTRACT

Pathogenic variants in the *Leucine-rich repeat kinase 2* (*LRRK2*) gene are a primary monogenic cause of Parkinson's disease (PD). However, the likelihood of developing PD with inherited *LRRK2* pathogenic variants differs (a phenomenon known as "reduced penetrance"), with factors including age and geographic region, highlighting a potential role for lifestyle and environmental factors in disease onset. To investigate this, household dust samples from four different groups of individuals were analyzed using metabolomics/exposomics and metagenomics approaches: PD+/LRRK2+ (PD patients with pathogenic *LRRK2* variants; n = 11), PD-/LRRK2+ (individuals with pathogenic *LRRK2* variants but without PD diagnosis; n = 8), iPD (PD of unknown cause; n = 11), and a matched, healthy control group (n = 11). The dust was complemented with metabolomics and lipidomics of matched serum samples, where available. A total of 1,003 chemicals and 163 metagenomic operational taxonomic units (mOTUs) were identified in the dust samples, of which ninety chemicals and ten mOTUs were statistically significant (ANOVA p-value < 0.05). Reduced levels of 2-benzothiazolesulfonic acid ($BThSO_3$) were found in the PD-/LRRK2+ group compared to the PD+/LRRK2+ . Among the significant chemicals tentatively identified in dust, two are hazardous chemical replacements: Bisphenol S (BPS), and perfluorobutane sulfonic acid (PFBuS). Furthermore, various lipids were found altered in serum including different lysophosphatidylethanolamines (LPEs), and lysophosphatidylcholines (LPCs), some with higher levels in the PD+/LRRK2+ group compared to the control group. A cellular study on isogenic neurons generated from a PD+/LRRK2+ patient demonstrated that BPS negatively impacts mitochondrial function, which is implicated in PD pathogenesis. This pilot study demonstrates how non-target metabolomics/exposomics analysis of indoor dust samples complemented with metagenomics can prioritize relevant chemicals that may be potential modifiers of *LRRK2* penetrance.

1. Introduction

Parkinson's disease (PD) is a neurodegenerative disorder, affecting 1.8 % of individuals over the age of 80 years globally, with an increasing prevalence due to the progressive aging of the population (Steinmetz, 2024). PD is characterized by the abnormal accumulation of misfolded

* Corresponding authors.
E-mail addresses: begona.talavera@uni.lu (B. Talavera Andújar), emma.schymanski@uni.lu (E.L. Schymanski).
[1] Shared senior authors: PW, CK, AG, ELS.

https://doi.org/10.1016/j.envint.2024.109151
Received 30 August 2024; Received in revised form 12 November 2024; Accepted 12 November 2024
Available online 16 November 2024

alpha-synuclein (α-syn) inside neurons, leading to the formation of Lewy Bodies, which promote neuroinflammation and the irreversible degeneration of dopaminergic neurons in the *substantia nigra pars compacta* and other brain regions (Chen and Lin, 2022; Vascellari, et al., 2020; Talavera Andújar, 2022; Lubomski et al., 2020). The clinical hallmarks of PD are tremor, bradykinesia, rigidity, and later in the disease, postural instability (Chen and Lin, 2022). However, these typical motor features do not become evident until 60–80 % of dopaminergic neurons are lost, such that other indicators are needed for earlier diagnosis (Bloem et al., 2021). Non-motor symptoms related to PD, such as constipation and REM-sleep behavior disorder (RBD), can occur decades before the onset of the classical motor symptoms but often go unrecognized (Chen and Lin, 2022; Lubomski et al., 2020; Bloem et al., 2021; Romano et al., 2021). Since not all PD patients have Lewy bodies or positive α-syn readings (Siderowf, 2023; Schneider and Alcalay, 2017), recently, a biological classification of PD has been proposed for research purposes, which considers the presence or absence of α-syn pathology, features of neurodegeneration, and genetic contributions (Höglinger, 2024).

Although the exact cause of most of patients with PD remains unknown, recent studies suggest that a combination of genetic and environmental risk factors may play a key role in the development of the disease (Chen and Lin, 2022; Bloem et al., 2021; Lim and Klein, 2024). Typically, monogenic PD comprises five dominantly inherited forms (*SNCA*, *LRRK2*, *VPS35, RAB32* and *CHCHD2*) and three recessively inherited forms (*PRKN*, *PINK1*, and *PARK7*) (Höglinger, 2024; Lim and Klein, 2024). Mitochondrial dysfunction may occur already in the early stages of PD pathogenesis and plays a crucial role in both sporadic and familial forms of the disease (Subramaniam and Chesselet, 2013; Bose and Beal, 2016). Gene variants of *Leucine-rich repeat kinase 2* (*LRRK2*) are the most common monogenic cause of PD, accounting for 1–2 % of all cases (Bjørklund et al., 2020; Trinh et al., 2022; Skrahina, 2021; Miller et al., 2024). Most of the *LRRK2* pathogenic variants result in increased kinase activity of the LRRK2 protein, leading to mitochondrial dysfunction and promoting inflammatory responses that may result in chronic neuroinflammation and gut inflammation (Chen and Lin, 2022; Trinh et al., 2022). In addition to PD, LRRK2 has been linked to inflammatory diseases including Crohn's Disease, leprosy and tuberculosis (Chen and Lin, 2022; Tsafaras and Baekelandt, 2022). While the p. G2019S pathogenic variant of *LRRK2* is the best known and most common, not all carriers of this variant will develop PD, a phenomenon termed "reduced penetrance" (Chen and Lin, 2022; Trinh et al., 2022; Usnich et al., 2021; Healy, 2008). Importantly, the penetrance is age-dependent and differs across geographic regions. For example, in Tunisia, 61 % of *LRRK2* p.G2019S carriers developed PD by the age of 60 years, and 86 % by the age of 70. In contrast, in Norway, only 20 % of carriers developed the disease by age 60, and 43 % by age 70 (Usnich et al., 2021; Hentati et al., 2014). This suggests that factors beyond genes, such as lifestyle or environment, may play a crucial role in triggering the onset of the disease (Chen and Lin, 2022). Various environmental factors have been previously associated with an increased risk of PD, including the exposure to metals (e.g., Cu, Fe and Zn) and pesticides (e.g., rotenone and paraquat) (Sakowski et al., 2024). In contrast, smoking, caffeine consumption, and the use of anti-inflammatory drugs have been linked with a reduced PD risk (Sakowski et al., 2024; Lüth, 2023). The LRRK2/Luebeck International Parkinson's Disease Study (LIPAD) cohort is one of the largest multinational cohorts of genetic PD, focused on LRRK2-associated PD and healthy *LRRK2* pathogenic variant carriers aiming to identify modifiers of *LRRK2* penetrance (Usnich et al., 2021). The present work describes a pilot study investigating the household dust from selected LIPAD cohort participants to determine whether this could potentially reveal potential chemical exposures and taxa of interest that may influence *LRRK2* penetrance, to help direct future sampling campaigns.

Although some chemicals have been found to positively or negatively impact PD development or progression (as described above), these were generally targeted studies and, thus, the effects of other chemical exposures on PD remain largely unknown. Since people in urban areas spend about 90 % of their time indoors (Shan et al., 2019), sampling the indoor environment offers a valuable opportunity to study both chemical and microbial exposures. Household dust can act as a reservoir of chemicals, with estimates ranging from 30,000 to 70,000 chemicals in household use (Schwarzenbach, 2006). With these numbers of chemicals, non-target analytical methods are required to explore which chemicals are present in household dust (Rostkowski, 2019; Hollender, 2023). In addition to chemicals, the gut microbiome has been proposed to play an important role in PD pathogenesis (Lubomski et al., 2020). The household dust microbiome can influence the host microbiome (Shan et al., 2019), linking indoor microbial exposures to potential health outcomes including via the oral-gut axis (Kunath et al., 2024). So far, between 500 and 1,000 different microbial species have been reported in dust (Shan et al., 2019; Thompson, et al., 2021). Consequently, the analysis of household dust is of great interest to generate new hypotheses about environmental factors contributing to the penetrance of PD.

As part of the LIPAD study (Usnich et al., 2021), this work aims to identify potential environmental modifiers of the penetrance of *LRRK2* pathogenic variants through the analysis of household dust of four groups of participants: PD+/LRRK2+ (PD individuals with pathogenic *LRRK2* variants), PD-/LRRK2+ (individuals with pathogenic *LRRK2* variants but without PD diagnosis), iPD (PD of unknown cause), and a matched control group (individuals without pathogenic variants and without PD diagnosis), through different metabolomics/exposomics and metagenomics approaches. This was complemented with non-target metabolomics on paired serum samples, where available, to investigate potential metabolomic differences between groups that could be attributed to environmental exposures. Additionally, since alterations in bile acids (BAs) have been previously noted in PD (Li, 2021; Graham, 2018; Loh, 2024), a target study of BAs in serum was performed. Finally, a cell study in isogenic neurons generated from a PD+/LRRK2+ patient was conducted to investigate the potential neurotoxic effects of a chemical found in the household dust, using various readouts related to mitochondrial function. To our knowledge, this is the first study investigating the environmental influences of *LRRK2* penetrance through the molecular analysis of household dust.

2. Material and methods

2.1. Sample collection

Samples from four different groups of individuals (Control, iPD, PD-/LRRK2+, PD+/LRRK2+, explained above) were collected in Germany (36) and Turkey (5) between February 2020 and January 2022, with details provided in Table 1. Additional information has already been published (Usnich et al., 2021). Participants with different *LRRK2* variants were included in this study. In the PD+/LRRK2+ group, seven

Table 1
Demographic characteristics of the studied groups (mean ± standard deviation). (a) ANOVA single factor was applied to calculate the p-value of the age across groups, while Chi-square p-value was computed for the categorical variable (sex).

Sample	Details	Control	iPD	PD-/ LRRK2+	PD+/ LRRK2+	p-value[(a)]
Dust	n	11	11	8	11	
	Age	60.54 ± 11.15	62.45 ± 7.88	50.75 ± 10.40	61.73 ± 8.33	0.0487
	Sex (f/m)	6/5	6/5	7/1	6/5	0.4012
Serum	n	8	3	8	5	
	Age	60.40 ± 9.27	65.00 ± 6.00	50.75 ± 10.40	58.20 ± 8.38	0.6864
	Sex (f/m)	5/3	3/0	7/1	1/4	0.0455

participants carried the p.G2019S variant, two had the p.N1437S variant, and one each had the p.R1441H and p.I2020T variants. In the PD-/LRRK2+ group, six individuals carried the p.G2019S variant, while one each had the p.R1441C and p.S901L variants. Importantly, carriers of pathogenic and likely pathogenic variants in 68 PD-linked genes were excluded in the iPD and control groups, as specified in the ROPAD protocol (Skrahina, 2021; Westenberger, 2024). Further details about the participants can be found in **Table S1**.

A total of forty-one dust samples were collected from vacuum cleaner bags stored at room temperature until analysis. To facilitate this, each participant was asked to provide a single sample, either their vacuum cleaner bag or household dust, which was securely placed in a plastic bag closed with a tight knot. The household dust samples were subsequently shipped at ambient temperature to the receiving laboratory. In addition, twenty-four matched serum samples were collected (Table 1) and stored at –80 °C until the analysis. Samples were matched by gender and age across the control, iPD, and PD+/LRRK2+ groups (Table 1). Matching the PD-/LRRK2+ group was more challenging due to the younger average age and the specific clinical characteristics of these participants. Fig. 1 shows the number of samples per group, and the analyses performed (described further in the following sections).

2.2. Sample preparation

2.2.1. Dust

The sample extraction protocol for metabolomics/exposomics was adapted from Moschet *et al.* (Moschet et al., 2018) and Dubocq *et al.* (Dubocq et al., 2021). Briefly, 50 mg of each dust sample was extracted using acetonitrile (ACN): methanol (MeOH) (1:1, v/v). The extract was evaporated (Labconco CentriVap, −4 °C, 24–48 h), reconstituted using 0.1 % formic acid (FA) in MilliQ water and MeOH (90:10, v/v), and filtered (Phenex-RC 4 mm syringe filter, 0.2 µm). Ten internal standards were used to check the instrument performance (see **Table S2**). Extraction blanks and pooled quality control (QC) samples were prepared following the guidelines from Broadhurst *et al.* (Broadhurst, 2018). Details about the pooled QC preparation are shown in **Figure S1**. A standard mix of 170 polar compounds (50 µM) was used to serve as reference standards later (see **Table S3** for full listing). Further details are given in the Supplementary Material (SM), section **S1.1.1**.

For the metagenomic analyses, 100 mg of each dust sample were aliquoted, and DNA was extracted using the DNeasy PowerLyzer PowerSoil Kit (Qiagen, 12855–50). Tests were performed at three input amounts (50 mg, 100 mg, and 150 mg), whereby 100 mg of material yielded the best output in terms of DNA concentrations and quality, see **S1.1.1** (**Figure S2-S3**) for details. The manufacturer's protocol was followed (DNeasy PowerLyzer PowerSoil Kit, 2024), with the exception that DNA extracts were eluted in 40 µL of sterile DNA-free PCR-grade water instead of 100 µL of Solution C6.

2.2.2. Serum

The protocol for the non-target LC-HRMS analysis was adapted from Cajka *et al.* (Cajka et al., 2017) and Lange *et al.* (Lange and Fedorova,

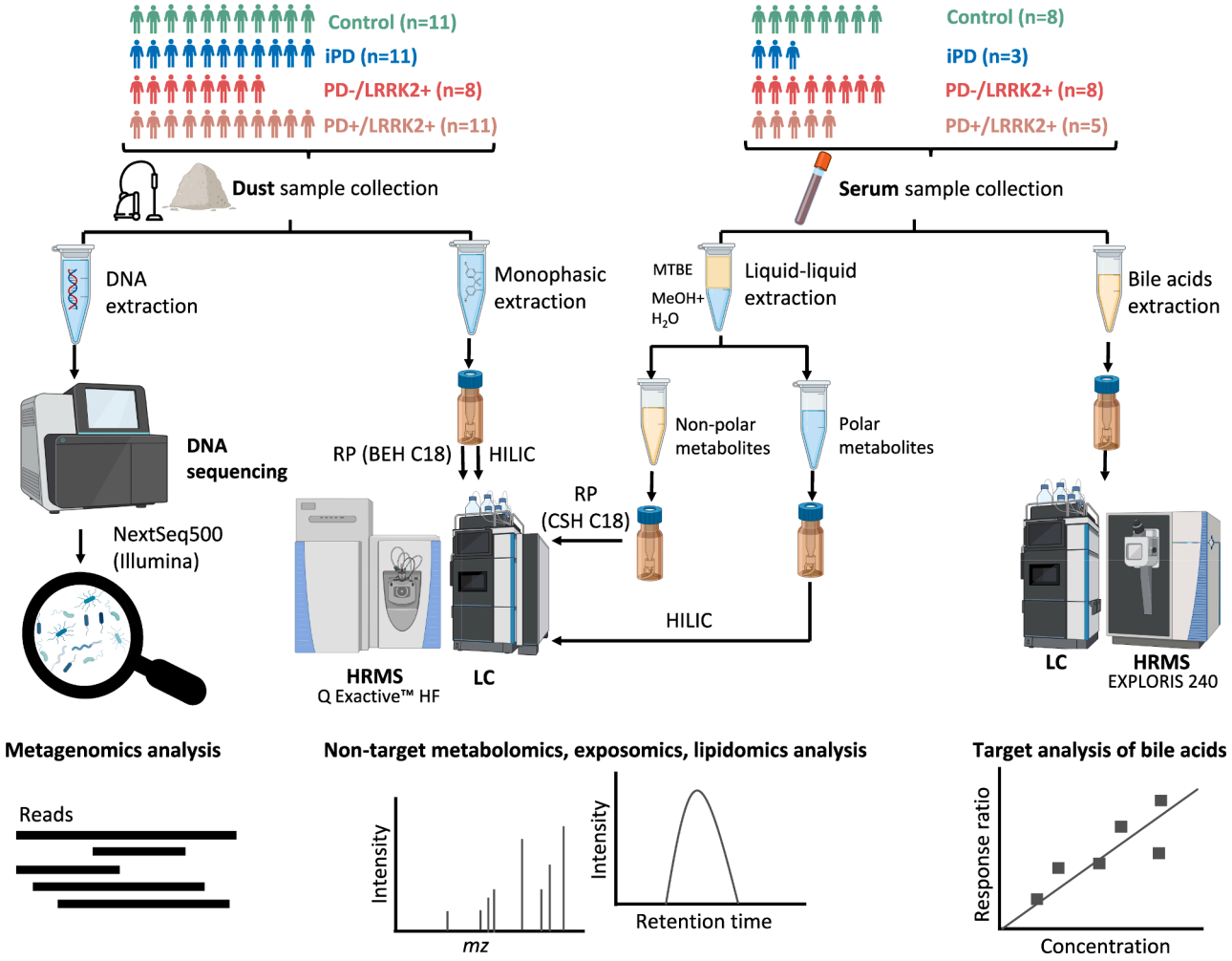

Fig. 1. Scheme showing the four groups under study, type of samples analyzed (dust and serum), as well as the different analyses performed in each of them. Note that all the serum samples were matched with the dust.

2020); detailed in full in **S1.1.2** and shown in **Figure S4**. Briefly, serum samples were thawed on ice and extracted via liquid–liquid extraction (LLE) with cold MeOH containing 14 SPLASH® LIPIDOMIX® mass spectrometry standards (listed in **Table S4**, chromatograms shown in **Figure S5-S6**), methyl *tert*-butyl ether (MTBE), containing cholesteryl ester 22:1 (CE22:1), and MilliQ water. The QC, extraction blank samples, and the standard polar mix of 170 compounds (**Table S3**) were as described for the dust samples.

For the targeted BA analysis, 50 µL of each serum sample was extracted with MilliQ water (containing four IS) and cold MeOH. The IS were cholic-D4 acid (CA-D4), deoxycholic-D4 acid (DCA-D4), lithocholic-D4 (LCA-D4), and glycocholic-D4 acid (GCA-D4). A mixture of fourteen targeted BAs (10 µg/mL) was prepared (listed in **Table S5**). This standard solution was further diluted step by step to build the calibration curve. Further details are given in **S1.1.2**.

2.3. Instrumental analysis

2.3.1. Metabolomics/Exposomics/Lipidomics

Non-target analysis of dust and serum was performed on a Thermo Scientific Accela LC system coupled to a Q Exactive™ HF (Thermo Scientific) mass spectrometer using electrospray ionization (ESI) in both positive (+) and negative (−) ionization modes. Dust samples were analyzed using an Acquity BEH C_{18} reversed phase (RP) column (150 × 2.1 mm; 1.7 µm), and a SeQuant® ZIC-pHILIC 5 µm polymer (HILIC) column (150 × 2.1 mm), each with the respective guard column. The HILIC method was also employed to analyze the polar extracts of the serum samples. The HRMS was operated in full scan profile mode with a scan range of 60–900 *m/z*. Complete details of the RP and HILIC LC-HRMS methods are given in Talavera Andújar *et al.* (Talavera Andújar, 2022).

The non-polar extracts of the serum samples were analyzed (lipidomics) with an RP method adapted from Cajka *et al.* (Cajka et al., 2017); using an Acquity UPLC CSH C_{18} RP column (100 × 2.1 mm; 1.7 µm) coupled to a guard column (130 Å, 1.7 µm, 2.1 mm X 5 mm). Full details are given in **S1.2.1**.

2.3.2. Target analysis of BAs

The target analysis of BAs (**Table S5**) was performed on a LC system coupled to a Thermo Orbitrap Exploris 240. The HRMS was operated in negative ionization mode (full scan mode) with a scan range of 100–620 *m/z*, with the same column as for the lipidomics analysis. Full details are given in **S1.2.2**.

2.3.3. Metagenomic analyses

DNA was quantified using Qubit fluorometer and Quant-iT dsDNA HS Assay kits to obtain accurate concentration values. A Nanodrop instrument was then employed to determine DNA quality through the 260/280 and 260/230 ratios (**Table S6**). DNA libraries were prepared after PCR amplification, taking the same starting DNA from each sample. 50 ng of DNA were used for metagenomic library preparation using the xGen DNA library preparation kit (Cat. no. 10009822, Integrated DNA Technologies) using xGen UDI-UMI adapters (Cat. no. 10005903). The genomic DNA was enzymatically fragmented for 10 min and DNA libraries were prepared with PCR amplification. The average insert size of libraries was 400 bp. Prepared libraries were quantified using Qubit (DNA HS kit, Thermo) and quality checked with DNA HS kit on Bioanalyzer 2100 (Agilent). Sequencing was performed at the LCSB Genomics Platform (RRID: SCR_021931) on NextSeq2000 (Illumina) instrument using 2x150 bp read length.

2.4. Data analysis

2.4.1. Metabolomics/Exposomics/Lipidomics

For the dust and serum (polar extracts), raw files (".raw") were converted to ".mzML" format using ProteoWizard MSConvert (Version 3.0.20331.3768aa6e9 64-bit) (Chambers, 2012). The converted files were analyzed with the open software patRoon (version 2.1.0) (Helmus et al., 2021; Helmus et al., 2022), using the non-target and suspect screening options. This was complemented with MS-DIAL (version 4.9.221218) (Tsugawa, et al., 2015) using version 17 of the MSP libraries; the MS-DIAL input parameters are given in **Table S7**. Further details are given in **S1.3.1** and **Figure S7**; the code for patRoon is available on GitLab (Andújar, 2024).

For the lipid analysis in serum, the LC-HRMS raw data files were processed in MS-DIAL (parameters given in **Table S8**) using the *in silico* LipidBlast (Kind et al., 2013) library. To complement the MS-DIAL lipid annotations, which are similarity-based, LipidMatch (Koelmel, 2017), a rule based software, was employed (see **Figure S8**). The annotations from MS-DIAL and LipidMatch were combined; LipidMatch annotations were selected in case of duplicates.

Among all features identified by non-target and suspect screening approaches in dust and serum, only those with MS/MS information and MS/MS match values were considered for further analysis and chemical annotation. R (version 4.1.2) via RStudio (version 2022.02.3) was used to filter the samples. Features with a relative standard deviation (RSD) $>$ 50 % in the QC-pooled samples were discarded. Since patRoon, MS-DIAL and LipidMatch use different approaches to annotate compounds and match MS/MS spectra, four different types of criteria were used to annotate confidence levels to the features (details given in **Table S9**). Note that only high confidence features, Level 1 to Level 3 (matching various criteria shown in **Table S9**), were considered in this study to ensure the quality of the biological interpretation. Features were annotated as Level 1 when the match between the chemical standard (**Table S3**) and tentative candidate (in the dust or serum) yielded a SpectrumSimilarity score $\geq$ 0.7 and the retention time (RT) shift was $<$ 1 min. *OrgMassSpecR* (Dodder and Mullen, 2017; Nontargeted Comprehensive Two-Dimensional Gas Chromatography/Time-of-Flight Mass Spectrometry Method and Software for Inventorying Persistent and Bioaccumulative Contaminants in Marine Environments, 2024) was used to calculate spectral similarity. Xcalibur Qual Browser (version 4.1.31.9) was used to check the RT and to extract the MS/MS information. The annotated chemicals were classified using the MetOrigin web server (Yu et al., 2022) and the PubChem Classification Browser (Kim, 2023), using both the PubChem Compound Table of Contents (TOC) (PubChem Classification Browser, 2024) and the NORMAN Suspect List Exchange (NORMAN-SLE) (PubChem Classification Browser, 2024) classification browsers. Chemical structures were generated using CDK Depict (Mayfield, 2023).

For the statistical analysis, peak intensity tables were uploaded to MetaboAnalyst 6.0 (web interface) (Pang, 2024), normalized by sum, $\log_{10}$ transformed and Pareto-scaled. Principal Component Analysis (PCA) was performed using MetaboAnalyst 6.0 while Analysis of Variance (ANOVA) with Tukey's honestly significant difference (HSD) post hoc test was computed in R (version 4.1.2). A p-value $<$ 0.05 was considered as statistically significant in this study. Significant lipids in serum were subsequently subjected to Lipid Pathway Enrichment Analysis (LIPEA) (LIPEA | What is LIPEA, 2024). Multiple linear regressions (lm function in R) were computed to investigate the relationship between the chemical levels (peak intensities) and clinical characteristics (**Table S1**).

For the target screening of BAs, concentrations of the detected BAs were calculated by interpolating the constructed IS-calibrated linear-regression curves of individual BAs, with the peak area ratios measured form injections of the sample solutions. TraceFinder 5.2 General Quan (Thermo) was employed for this analysis. GraphPad Prism (version 10.1.0) was used to perform ANOVA with Tukey's HSD and graphs.

2.4.2. Metagenomic analyses and omics integration

The Integrated Meta-omic Pipeline (Narayanasamy, 2016) (IMP; v3.0 commit# 9672c874; available at GitLab (Narayanasamy et al., 2024) was employed to process paired and reverse reads using the

metagenomic workflow with default settings. As part of the workflow, metagenomic reads aligning with the human genome were filtered and removed. Taxonomic profiles were generated using mOTUs (v2.0). Furthermore, reads were assembled into contigs, which were used for gene predictions using Prokka (Seemann, 2014), and subsequently annotated using the Kyoto Encyclopedia of Genes and Genomes (KEGG) orthologous categories. The KEGG orthologous (KO) genes were identified, and their coverages based on number of reads mapping to individual KOs were used for subsequently analyses.

The mOTU table was normalized by the total sequence count following which MicrobiomeAnalyst 2.0 (Chong et al., 2020; Lu et al., 2023), marker data profiling option, was employed to filter based on a prevalence threshold of 30 % across samples (minimum count requirement of one), and to compute alpha-diversity and core microbiome composition. In addition, the ampvis2 (Andersen, 2024) R package was employed for data visualization purposes. As for the metabolomics/exposomics data, ANOVA test was computed in R and a p-value < 0.05 was considered statistically significant.

For the KOs, Transcripts Per Kilobase Million (TPM) were calculated in R, accounting for sequencing depth per sample and gene lengths. Pathways from the significant KOs were obtained via the KEGGREST (KEGGREST, 2024) package in R, see the GitLab repository for details (Andújar, 2024). To provide a comprehensive overview, TPM values of KOs sharing the same pathway were summed and ANOVA was performed to identify the statistically significant pathways across groups.

The normalized abundance mOTU table (metagenomics) and normalized peak intensities table (metabolomics/exposomics) were integrated using Data Integration Analysis for Biomarker discovery using latent components (DIABLO) within the mixOmics (Rohart et al., 2017) package in R. Details about this analysis are available in the GitLab repository (Andújar, 2024). Spearman's correlation between the mOTUs and chemicals was computed in R, using the cor.test function of the base R stats package, while the Corrplot package, was used to perform the correlation plots.

The MultiGroupPower function from the MultiPower R package (ConesaLab, 2024; Tarazona, 2020) was applied to compute the power calculations integrating the metabolomic/exposomic and metagenomic datasets, derived from the dust analysis.

2.5. Neuronal differentiation and bisphenol s (BPS) exposure

2.5.1. Generation of midbrain dopaminergic neurons

Induced pluripotent stem cells (iPSCs) were obtained from a PD individual carrying the *LRRK2* G2019S variant. An isogenic control (IC) was engineered from the same line using CRISPR-Cas9 technology (Qing et al., 2017; Reinhardt, 2013; Nickels, 2019). Neuronal cultures enriched in midbrain dopaminergic neurons were generated following the Reinhardt *et al.* protocol (Reinhardt, 2013; Reinhardt, 2013), details can be found in **S1.4.1** and **Table S10.** At day 29, cells were treated for 24 h with bisphenol S (BPS) (Sigma, 43034), at two different concentrations (100 μM and 500 μM), using dimethyl sulfoxide (DMSO) (Sigma, D2438) as a vehicle, before staining and imaging. Details about the mitochondrial membrane potential and mitophagy assays can be found in **S1.4.2** and **S1.4.3**, respectively.

2.5.2. Image analysis

Automated image analysis was performed using Matlab (version 2021a, MathWorks), adapting the method detailed in Baumuratov *et al.* (Baumuratov, 2016). The analysis was performed on the HPC platform (Homepage | HPC @ Uni.lu, 2024) from the University of Luxembourg in collaboration with the LCSB Bioimaging platform. Features such as *mitochondrial mass* (sum of mitochondrial pixels/sum of nuclei pixels), *mitochondrial size* (sum of mitochondrial pixels/mitochondrial counts), *mitochondrial membrane potential* (mean intensity of TMRE inside the mitochondrial mask), and *normalized mitophagy* (sum of pixels positive for Mitotracker Green FM and Lysotracker Deep Red/sum of mitochondrial pixels) were extracted.

Statistical analyses and data visualization were performed in GraphPad Prism (version 10.1.0). Comparative analyses were performed using the Kruskal-Wallis test, followed by multiple comparisons with the uncorrected Dunn's test.

3. Results and discussion

3.1. Dust metabolome and exposome

3.1.1. Overview of chemical composition

The chemical composition of the dust was analyzed by non-target LC-HRMS, using the different cheminformatic approaches described above, resulting in 1,003 annotated chemicals (Level 1–3), with ninety features being statistically significantly different (ANOVA p-value < 0.05). PCA was performed to investigate the chemical composition across countries, with **Figure S9A** revealing no clear differences between Germany and Turkey. **Table S11** contains detailed information about all annotations, including statistical results and MetOrigin classifications, while **Table S12** contains the statistically significant chemicals only. The potential sources of these compounds according to the NORMAN-SLE (NORMAN Network | NORMAN, 2024) and PubChem Compound TOC (Kim, 2023) are shown in Fig. 2, while the MetOrigin (Yu et al., 2022) classifications are shown in **Figure S10**.

Hundreds of chemicals (784) in dust were found in different lists from the NORMAN-SLE tree (Fig. 2**A**). These NORMAN-SLE lists were selected to provide a comprehensive understanding of the types of chemicals annotated in the household dust samples. Most matches (544, of which 51 were significant) were found in the S32 REACH17 (Alygizakis and Slobodnik, 2018), which is a list of chemicals registered under REACH, the European Chemical Legislation that requires registration of chemicals in use above one tonne per annum (Lilienblum, 2008). Benzocaine, benzyl butyl phthalate, and scopoletin are some examples of REACH chemicals found in household dust samples. Notably, 204 out of the 1,003 chemicals identified in this study were previously noted in the NORMAN collaborative household dust trial (Rostkowski, 2019) (S35 INDOORCT16 list (Haglund and Rostkowski, 2016)). These included plasticizers such as dibutyl phthalate, pharmaceuticals such as tramadol, benzocaine, ketoprofen, gabapentin and the fungicide carbendazim, one of the most prevalent biocides in Italian household dust samples (Salis, 2017). Furthermore, 151 chemicals were potential ingredients of cosmetics, mapping to the S13 EUCOSMETICS (von der Ohe and Aalizadeh, 2000) list, while 52 were present in the list of chemicals associated with neurotoxicity (S37 LITMINEDNEURO (Baker et al., 2019)), including 2,4-dinitrophenol and diethyltoluamide (DEET). Additionally, 89 chemicals associated with plastic packaging (via S49 CPPDBLISTB list (Groh and Schymanski, 2019) were tentatively identified, including dibutyl phthalate, and bisphenol A diglycidyl ether. The overlap of chemicals across all these lists was high (Fig. 2**B**), suggesting that most of the annotated compounds have multiple potential origins and/or reasons for interest.

Fig. 2**C** shows the potential categories of chemicals based on the PubChem Compound TOC, with overlap in Fig. 2**D**. The "Use and manufacturing" category was the most prevalent, with such information available for 549 of the annotated compounds. Disorders and diseases information was associated with 453 compounds, including 4-chloro-3-methylphenol and DEET. Interestingly, 432chemicals were classified as food by the PubChem Compound TOC (Fig. 2 **C**), while 506 chemicals were in this MetOrigin class (**Figure S10A**); 366 of these overlapped. Additionally, 282chemicals are potentially related to microbiota according to MetOrigin (**Figure S10A**). As for the NORMAN-SLE categories (Fig. 2**B**), the overlap across the different PubChem TOC categories was high (Fig. 2**D**).

3.1.1.1. Relevant chemicals potentially related to penetrance. Ninety

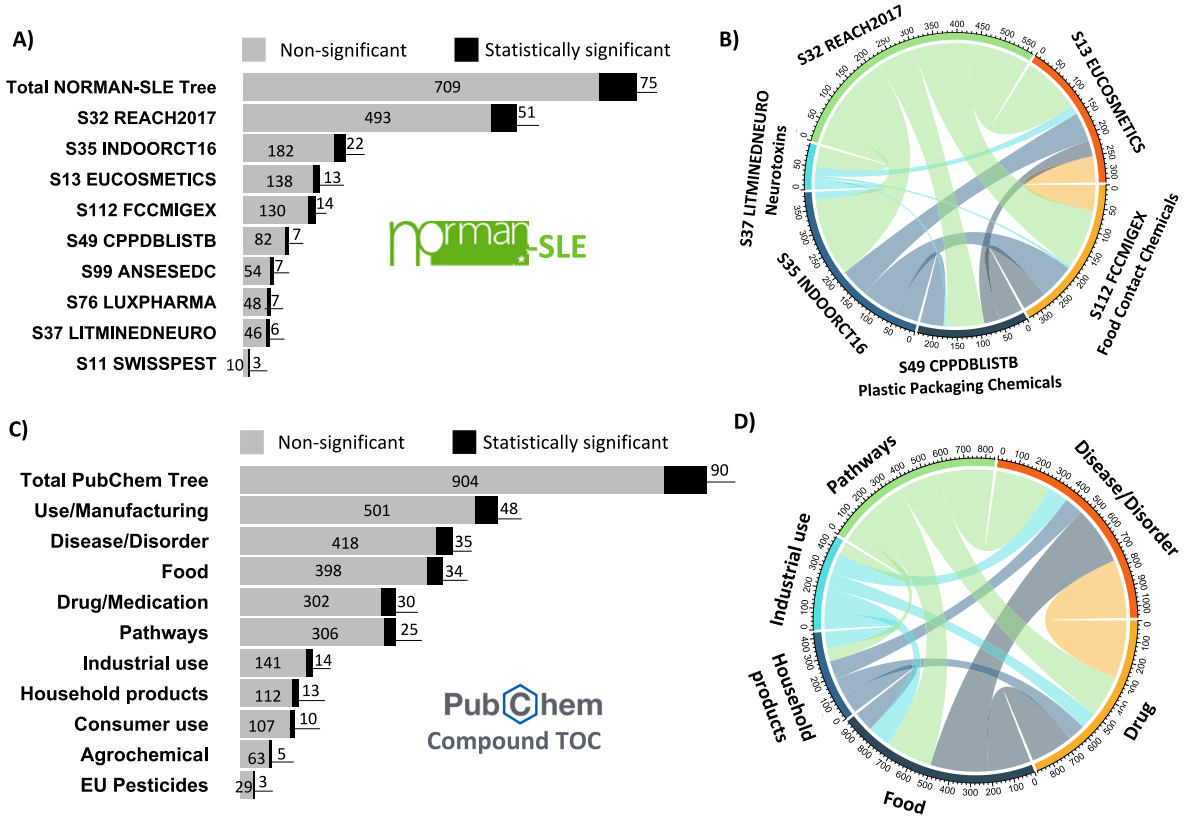

Fig. 2. Potential sources of the identified chemicals in the dust. **(A)** Selected lists from the NORMAN-SLE tree; **(B)** Chord diagram displaying the overlap of the different lists; **(C)** Selected categories from the PubChem TOC; **(D)** Chord diagram displaying the overlap of different PubChem categories **(D).** Statistically significant refers to features with ANOVA p-value < 0.05. Full results are available in **Table S11**. Note that queriers were performed in April 2024.

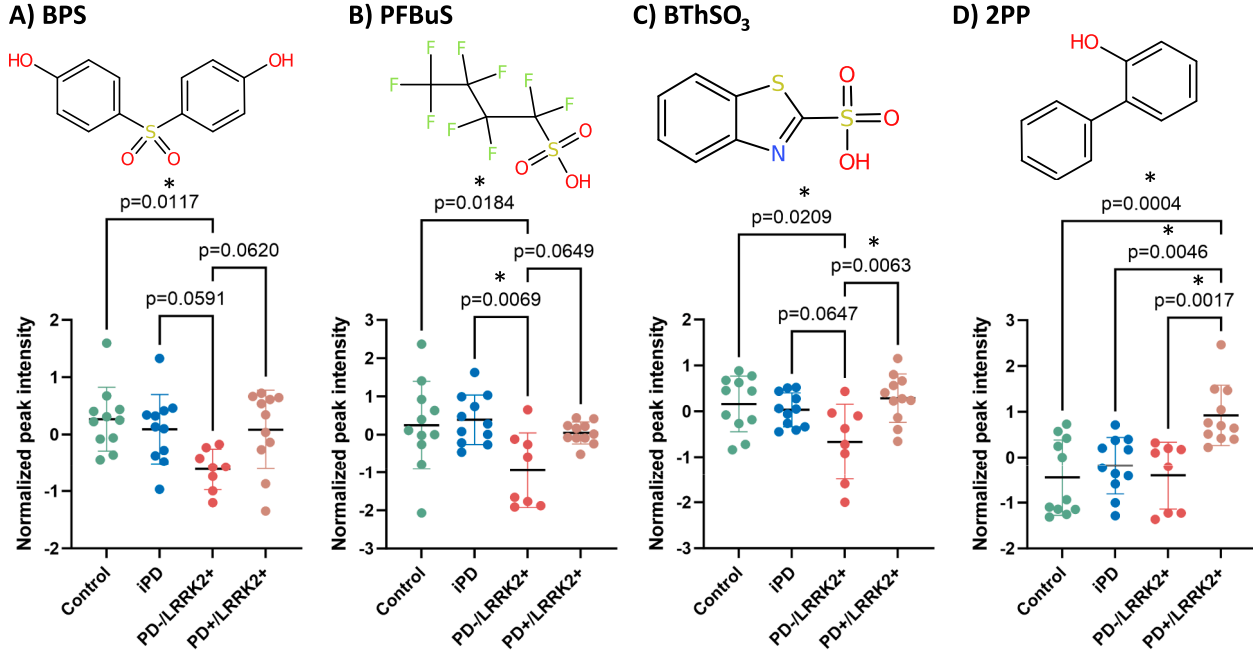

Fig. 3. Normalized peak intensities across groups of **(A)** BPS; bisphenol S, **(B)** PFBuS; perfluorobutane sulfonic acid, **(C)** $BThSO_3$; 2-Benzothiazolesulfonic acid, and **(D)** 2PP; 2-phenylphenol in dust. p = Tukey's HSD post-hoc p-value. Note that p < 0.1 is displayed although only p < 0.05 is considered statistically significant here (marked with an "*").

statistically significant chemicals were found across the groups, indicating potential relevance for disease penetrance. Fig. 3 shows the distribution of four of these: bisphenol S (BPS), perfluorobutane sulfonic acid (PFBuS), 2-benzothiazolesulfonic acid ($BThSO_3$) and 2-phenylphenol (2PP), all annotated as Level 2a. Additional information regarding the MS/MS matches with the spectral library are provided in **Figure S11** and **Table S13**. Interestingly, the first two are replacements of hazardous chemicals; BPS (Fig. 3**A**) emerged as a "safer" alternative to bisphenol A (BPA) (Naderi and Kwong, 2020), while PFBuS (Fig. 3**B**) is a substitute for perfluorooctane sulfonate (PFOS) (Hu et al., 2022). All compounds illustrated in Fig. 3 had elevated levels in PD+/LRRK2+ compared to the PD-/LRRK2+ group. Thus, these compounds could be potential targets for further investigations into environmental influences on *LRRK2* penetrance in PD.

Significantly higher levels of BPS were found in the control group compared to the PD-/LRRK2+ . Higher levels of BPS were also observed in the PD+/LRRK2+ group compared to the PD-/LRRK2+ group (Fig. 3**A**). Two other bisphenol species, bisphenol P and bisphenol A diglycidyl ether (**Figure S12**), were also annotated in the dust samples, albeit not found to be statistically significantly different. BPS has been employed extensively in industry to produce BPA-free products. However, BPS can have similar or even greater toxicity than BPA (Gyimah, 2021), exhibiting stronger reproductive effects, DNA damage, longer bioavailability, and better dermal penetration compared with BPA (An et al., 2021). Additionally, BPS exhibits higher resistance to biodegradation, rendering it more prone to accumulate and persist in the environment (Naderi and Kwong, 2020). It can disrupt lipid metabolism, glucose metabolism, nucleotide metabolism, vitamin metabolism, and induce oxidative stress (An et al., 2021). BPS can cross the blood brain barrier (BBB) (Schirmer et al., 2021) and may trigger neurotoxicity through different pathways, potentially posing a risk factor for the development of neurodegenerative diseases including PD (Naderi and Kwong, 2020; An et al., 2021). Therefore, this compound was tested in cell-based models (neurons), to investigate its potential neurotoxic effects, as discussed in **Section 3.5**.

The dust analysis revealed significantly lower levels of PFBuS (Fig. 3**B**) in the PD-/LRRK2+ participants compared to the iPD and control groups, while a similar lower trend was found in PD-/LRRK2+ group compared with PD+/LRRK2+ . PFBuS is a per-/polyfluoroalkyl substance (PFAS), which is a group of substances of high environmental and toxicological concern due to their long-term environmental persistence and toxicity to organisms, including humans (Cousins, 2020). PFBuS, a relatively short-chain PFAS, is currently used as substitute for PFOS due to lower toxicity and bioaccumulation (Hu et al., 2022; Min, 2023). However, adverse effects including cytotoxicity, endocrine disruption, immunotoxicity, reproductive toxicity, hepatotoxicity and neurotoxicity have been associated with PFBuS (Hu et al., 2022; Min, 2023). PFBuS can cross the BBB, affecting the Central Nervous System (CNS). While PFBuS is considered less toxic than PFOS, both compounds exhibited similar mechanisms of toxicity in zebrafish models (Min, 2023).

Ten additional PFAS were annotated in dust, including the pesticide fipronil and its transformation products fipronil desulfinyl and flipronil sulfone, which were mainly found in one patient from the iPD group (**Figure S13A-C**). Fipronil, a PFAS-containing pesticide subject to stringent regulations in Europe due to its potential environmental and health-related risks, was (unexpectedly) identified in the dust samples. Although the use of fipronil in food production for human consumption was banned in Europe in 2013, eggs contaminated with fipronil were found in the Netherlands and neighboring countries in 2017 (van der Merwe et al., 2019; Kathage et al., 2018). The veterinary application of fipronil emerged as a significant potential source of this compound in household dust across Europe. Nonetheless, a prior study conducted in Italy in 2016 noted that the highest levels of fipronil were observed in a household dust without pets (Testa et al., 2019). These findings, coupled with our observation of fipronil in German household dust, underscore the necessity for continued regulatory interventions in Europe. Fluometuron (**Figure S13D**), another PFAS-containing pesticide, was also tentatively identified with overall higher peak intensities in the PD-/LRRK2+ dust samples. Additionally, PFAS-containing pharmaceuticals were annotated, including fluoxetine, flutamide, and etofenamate, without significant differences across groups (**Figure S14**). A PFAS with multiple industrial uses, 6:2 fluorotelomer sulfonic acid (6:2 FTSA), had a non-significant lower trend in the PD-/LRRK2+ group compared to the control (**Figure S15A**). Trifluoromethanesulfonic acid (TFMS), an ultra-short chain PFAS, showed statistically higher levels in the dust from the PD+/LRRK2+ group compared to the PD-/LRRK2+ (**Figure S15B**).

2-Benzothiazolesulfonic acid ($BThSO_3$) was found at statistically significantly lower levels in the PD-/LRRK2+ group compared to the PD+/LRRK2+ (Fig. 3**C**). This trend was also consistent with its transformation product, 2-hydroxybenzothiazole (OBTh), as shown in **Figure S16A**. Benzothiazole (BTh), a parent compound of OBTh, 2-(4-morpholinyl)benzothiazole (24MoBTh), and 2-aminobenzothiazole (ABhT) were also detected in the dust samples, without being statistically significantly different (**Figure S16B-D**). Benzothiazoles (BThs) have multiple applications, including as vulcanization accelerators in rubber manufacture, fungicides, antialgal agents, slimicides, chemotherapeutics and corrosion inhibitors (De Wever et al., 2001). BThs undergo chemical, biological and photodegradation in the environment, leading to the formation of several transformation products (Liao et al., 2018), as shown in **Figure S17** and discussed later (**Section 3.3**). Previous studies have associated BThs with different toxic effects, including carcinogenicity (Liao et al., 2018; Gu et al., 2024; Hornung, 2015) and impaired child neurodevelopment due to prenatal exposure (Cao, 2023). However, the environmental exposure to these compounds and the long-term consequences are presently unresolved.

2-Phenylphenol (2PP), an antimicrobial agent used in household products and included in the European Union pesticides database, was found with statistically significantly higher levels in the PD+/LRRK2+ group compared with the three others (Fig. 3**D**). 2PP was previously found in household waste (Nielsen et al., 2023), food and dairy products (Palacios Colón et al., 2021) and cosmetics (S13 EUCOSMETICS list (von der Ohe and Aalizadeh, 2000), as illustrated in Fig. 2**A**). It is also listed as a potential endocrine disruptor in the S109 PARCEDC list of potential endocrine disrupting compounds (Andres and Dulio, 2024). Moreover, a recent rat-based study showed that the exposure to this compound altered phospholipid, fatty acids, sterol lipid, and amino acid levels (Nazar, 2024).

The relationship between these four chemicals (Fig. 3) and various clinical and lifestyle characteristics of the individuals was explored (**Figure S18**). The analysis revealed that higher consumption rates of meat and fish were significantly and positively correlated with elevated levels of BPS and PFBuS in household dust, respectively. Importantly, correlation does not imply causation, and there could be other confounding factors affecting the chemical levels. Moreover, since the sample size was small, and complete information was not available for all the participants (**Table S1**), these findings should be interpreted with caution and further validated in a larger cohort of patients. Further details about the analysis are available in the GitLab repository (Andújar, 2024).

While four chemicals have been discussed in more detail here due to their relevance as potential neurotoxic compounds in the environment and for space reasons, another 86 compounds were found to be statistically significant across groups, as detailed in **Table S12**.

3.2. *Differentially abundant taxa and microbial gene Signatures*

To complement the dust-derived metabolomics/exposomics, the microbial communities of the dust samples were analyzed at different taxonomic ranks (from kingdom to species). A total of 1,782 metagenomic operational taxonomic units (mOTUs) were initially characterized (**Table S14**). PCA analysis was performed to explore the

variation in microbial composition across countries, but no major differences were observed (**Figure S9B**). This initial list was reduced to 163 mOTUs for subsequent analysis (**Table S15**), after filtering to remove low quality or uninformative features, as indicated in the Material and Methods section. Notably, *Actinobacteria*, *Proteobacteria,* and *Firmicutes* emerged as the three most abundant phyla (Fig. 4**A**). The dominance of these phyla in household dust aligns with multiple previous studies (Moschet et al., 2018; Shan, 2020; Thompson, et al., 2021). *Actinobacteria* spp., one of the most prevalent bacteria in house dust (Shan et al., 2019), were found with the highest abundance in the iPD dust samples, matching observations in previous studies showing this genus to be enriched in feces from PD patients (Vascellari, et al., 2020; Boktor, 2023).

The core microbiome at the species level was investigated (Fig. 4**B**), with *Cutibacterium acnes* the most prevalent species. This shows the significant biological components of the dust, including skin cells. Interestingly, lower alpha-diversity was noted in the iPD group (phylum level) compared to the control group (Fig. 4**C-D**). However, no statistically significant differences were observed in the alpha-diversity at species level (**Figure S19**), aligning with previous studies which reported no significant differences in the alpha-diversity in the feces of PD patients compared to the control participants (Vascellari, et al., 2020; Boktor, 2023).

Ten mOTUs were differentially abundant across groups ($p < 0.05$, ANOVA; **Table S15** and **Figure S20**), including *Clavibacter michiganensis, Marmoricola* sp. *Leaf446*, three different species of *Nocardioides* and *Sphingomonas, Candidatus Rickettsiella isopodorum,* and *Acinetobacter parvus*. Intriguingly, for all these mOTUS, the PD-/LRRK2+ group showed the lowest abundances. *Clavibacter michiganensis* (**Figure S20A**), recognized as a plant pathogen (Eichenlaub and Gartemann, 2011) (Pereira et al., 2017), demonstrated a significant increase in the iPD group compared to the control and PD-/LRRK2+ groups. The same trend was observed for *Marmoricola sp Leaf446.* (**Figure S20B).** This species has been mainly isolated from environmental sources, however a previous study found the *Marmoricola* genus to be highly abundant in the nasal microbiota of PD patients compared to control individuals (Pereira et al., 2017). *Nocardioides* (**Figure S20C-E**), was found elevated in the iPD group compared to the PD-/LRRK2+ . Of note, *Nocardioides* spp. can degrade a wide range of organic pollutants such as nitrophenol, ibuprofen, cotinine, melamine, or atrazine. Furthermore, *Nocardioides* can carry out steroid biodegradation and biotransformation (Ma, et al., 2023). *Sphingomonas* spp. (**Figure S20F-H**), was found significantly higher in the dust samples from the iPD compared to the PD-/LRRK2+ group. Interestingly, a previous study reported higher abundances of *Sphingomonas* genera in feces samples from PD patients, compared to a healthy control group, associated this with motor complications (Qian, 2018). *Candidatus Rickettsiella isopodorum* (**Figure S20I**), an intracellular bacterium infecting terrestrial isopods (Kleespies et al., 2014), was significantly higher in the control group. Lastly, statistically significantly elevated abundances of *Acinetobacter parvus* (**Figure S20J**) were observed in the PD+/LRRK2+ group compared to the others. This is an opportunistic pathogen associated with nosocomial infections.

In addition to the differentially abundant taxa, a total of 14,444 different KOs were characterized, of which 624 were statistically significant across groups. Pathways from the significant KOs were obtained, resulting in 269 KEGG pathways (**Table S16**) of which 207 were statistically significant. Fig. 5 illustrates the distribution of some of those pathways across groups, whereby the top thirty statistically significant pathways are represented in **Figure S21**. Notably, "microbial metabolism in diverse environment", "carbon metabolism" and "glyoxylate and dicarboxylate metabolism" pathways were increased compared to the control and iPD groups, compared to the PD-/LRRK2+ and PD+/

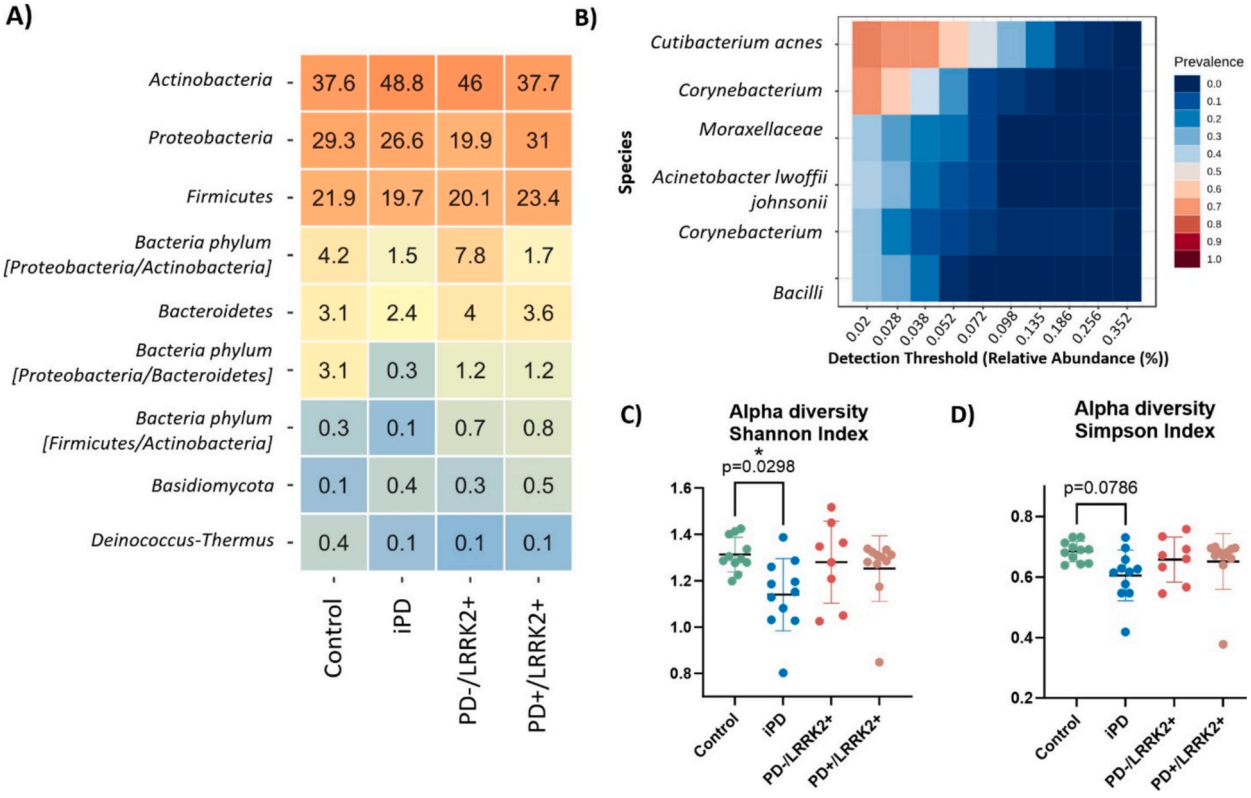

Fig. 4. (A) Heatmap showing the most abundant phyla entries from the "Phylum" column of the filtered mOTUS (**Table S15**). **(B)** Core microbiome showing the most abundant species entries from the "Species" column (**Table S15**). **(C)** Box plot showing the alpha-diversity across groups with Shannon Index and **(D)** Simpson Index at phylum level. p = Tukey's HSD post-hoc p-value. Note that $p < 0.1$ is displayed although only $p < 0.05$ is considered statistically significant here (marked with an "*").

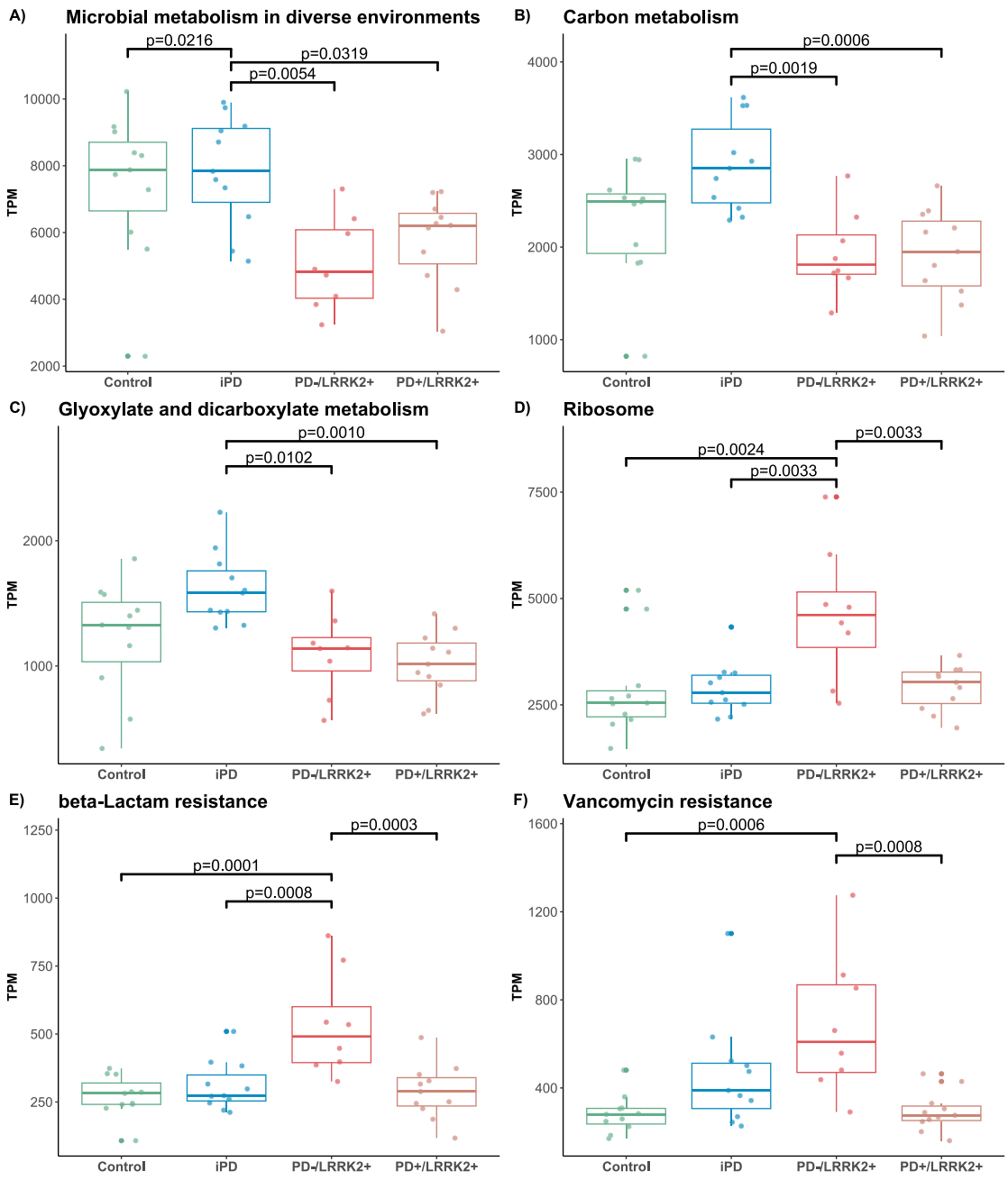

Fig. 5. Bar plots of some of the significant KEGG pathways found in the dust samples. Note that TPM values of the KOs sharing the same pathway were summed. p = Tukey's HSD post-hoc p-value. Abbreviations: TPM; Transcripts Per Kilobase Million, KOs; KEGG orthologous genes.

LRRK2+ groups (Fig. 5**A-C**). Furthermore, arginine, proline, phenylalanine, and butanoate metabolism exhibited the same trend, *i.e.*, significatively decreased in PD-/LRRK2+ compared to the control and iPD groups (**Figure S22**). In contrast, an increase in ribosomal genes was observed in PD-/LRRK2+ and PD+/LRRK2+ groups, suggesting that dust-borne bacteria might be compensating the lower metabolism (Fig. 5**D**). Finally, both beta-lactam and vancomycin resistance appear to be elevated in PD-/LRRK2+ and PD+/LRRK2+ (Fig. 5**E-F**). Overall, the pathways results (Fig. 5) show similar trends between control and iPD groups, and between PD-/LRRK2+ and PD+/LRRK2+ .

3.3. Dust omics Integration

Two different approaches were employed to investigate the potential relationships between the chemicals and the microbiome constituents found in the household dust: (1) DIABLO, a framework used to integrate the datasets of chemicals (**Table S11**), and mOTUs (**Table S15**) (Fig. 6**A-B**); and (2) Spearman correlation analysis, employed to explore in detail the potential correlation between some genera (*Rhodococcus* spp., *Pseudomonas* spp., and *Arthrobacter* spp.) and benzothiazoles (Fig. 6**C**). The DIABLO analysis (Fig. 6**A**) indicated that PD-/LRRK2+ clustered separately from the rest of the groups (left), while some iPD and control samples cluster together (right). This classification is mainly driven by the metabolomics/exposomics data, as most of the selected features are chemicals. Interestingly, two of the selected features are PFAS, PFBuS and 6:2 FTSA, which have lower levels in the PD-/LRRK2+ group compared to the controls, as previously indicated (Fig. 3**B** and **Figure S15A**). Sample plots from the final DIABLO model in Fig. 6**B** display the degree of agreement between the two datasets. Importantly, the PD-/LRRK2+ samples clustered together in both metabolomics and

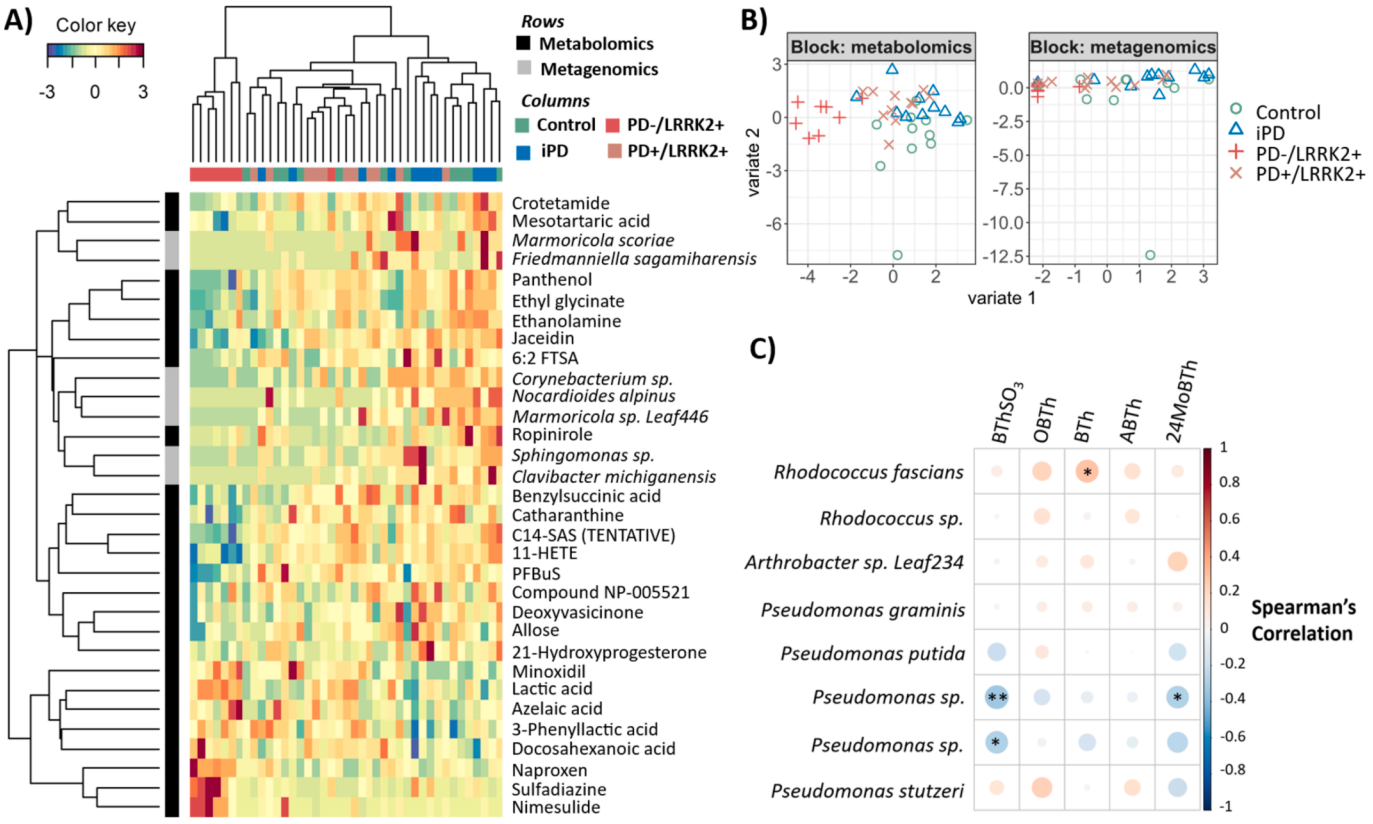

Fig. 6. **(A)** DIABLO Clustered heatmap showing the variables selected by multiblock sPLS-DA performed on the metagenomics (mOTUs table) and metabolomics/exposomics (peak intensities table) dust datasets on component 1. Samples represented in columns and features in rows. **(B)** DIABLO sample plot showing the discrimination across groups based on metabolomics (left panel) and metagenomics data (right panel). **(C)** Spearman's correlation analysis between Rhodococcus spp. and benzothiazoles. Red color indicates positive correlation while blue color indicates negative correlation. The size of the dots is proportional to the absolute value of the correlation coefficient. ** p-value < 0.05 *p-value < 0.1. Abbreviations: 6:2 FTSA; 6:2 fluorotelomer sulfonic acid, PFBuS; perfluorobutane sulfonic acid, $BThSO_3$; 2-Benzothiazolesulfonic acid, OBTh; 2-hydroxybenzothiazole, BTh; benzothiazole, ABTh; 2-Aminobenzothiazole, and 24MoBTh; 2-(4-Morpholinyl)benzothiazole. (For interpretation of the references to color in this figure legend, the reader is referred to the web version of this article.)

metagenomics datasets.

Certain species within the genus *Rhodococcus* have been reported to degrade $BThSO_3$ (Fig. 3**C**) to OBhT (**Figure S17**) (De Wever et al., 2001; Liao et al., 2018). Furthermore, BTh can be degraded by several bacterial species including *Rhodococcus* sp., *Pseudomonas* sp., *Arthrobacter* sp. and *Enterobacter* sp. (Liao et al., 2018). Interestingly, all of these were identified in the dust samples, although only the first three species were included in the filtered dataset (**Table S15**).

Spearman's correlation analysis was subsequently performed between all the BThs identified in the dust samples (Fig. 3**C** and **Figure S16**), and *Rhodococcus, Pseudomonas,* and *Arthrobacter* species, known for their capacity to degrade specific BThs (De Wever et al., 2001; Liao et al., 2018). A negative and statistically significant association was observed between *Pseudomonas* sp. and $BThSO_3$ (Fig. 6**C**). The same negative association was found between *Pseudomonas* sp. and 24MoBTh, suggesting that this species may degrade both $BThSO_3$ and 24MoBTh. Intriguingly, our analysis unveiled a positive (p-value < 0.1) association between BTh and *Rhodococcus fascians*. This association may be explained by several factors, including photodegradation or microbial degradation (e.g., by *Pseudomonas*) of other compounds such as 24MoBTh leading to the formation of BTh. Additionally, the presence of multiple microorganisms and chemicals in the household dust samples may influence the growth of *Rhodococcus fascians* and/or BTh metabolism. Therefore, further studies in controlled environments are necessary to provide more insights into the relationship between *Rhodococcus fascians* and BTh in household dust samples.

Overall, these results demonstrate agreement between both omics approaches as they effectively discriminated the same group (PD-/LRRK2+). Furthermore, the findings suggest a potential relationship between chemicals and microbes, indicating that some of the chemicals found in dust may be metabolized by microbes.

3.4. Serum Metabolome, Exposome, and lipidome

The analysis of dust samples was complemented by exploring the serum of some participants where matched samples were available. This included a non-target screening of polar chemicals (**Table S17**) and lipids (**Table S18-19**), as well as the quantitative target screening of BAs (**Table S20**).

3.4.1. Polar chemicals in serum

Forty-nine chemicals were annotated (Level 1–3) in the polar fraction of the serum samples, with three statistically significant results (1,7-dimethyluric acid, pipecolic acid, and amantadine). After data normalization, the PCA plot (**Figure S23**) displayed all the QC samples with a tight clustering. This indicates that the instrument variation was effectively corrected, affirming a good system stability and reliability of the results.

1,7-Dimethyluric acid, a metabolite of caffeine, was elevated in the control and PD-/LRRK2+ groups compared with the PD+/LRRK2+ group. Although this metabolite was not found in the dust, the parent compound (caffeine) was identified, without significant differences but with an average higher normalized peak intensity in the control group (**Figure S24**). These results agree with previous studies (Takeshige-Amano, 2020; Fujimaki, et al., 2018), which proposed lower levels of caffeine and caffeine metabolites as potential diagnostic biomarkers for

early PD. Caffeine, a common psychostimulant, has shown neuroprotective effects (via reduction of Reactive Oxygen Species (ROS)) and appears to improve motor symptoms in PD (Takeshige-Amano, 2020; Fujimaki, et al., 2018). Lower levels of caffeine and its metabolites in PD patients might be explained by a malabsoption in the small intestine. Although microbiome dysbiosis is a common feature in PD, to date it remains unclear whether caffeine malabsorption in PD is influenced by this (Fujimaki, et al., 2018).

Pipecolic acid was found significantly lower in the PD+/LRRK2+ group compared to the iPD group. This compound was also identified in the dust samples, without being statistically significantly different (**Figure S25**). Interestingly, opposite trends were observed, which suggests that biological samples do not always reflect environmental exposures. A previous study reported decreased levels of pipecolic acid in plasma samples from pre-PD individuals, suggesting that this may be indicative of microbiota-gut-brain axis (MGBA) dysregulation (Gonzalez-Riano, 2021). Pipecolic acid can be produced by intestinal bacteria and cross the BBB (Matsuda et al., 1995), where it can act as a neurotransmitter, modulating the uptake of γ-aminobutyric acid (GABA) by brain neurons (Gonzalez-Riano, 2021; Dalazen, 2014). Moreover, pipecolic acid may originate from the breakdown of lysine in human mitochondria and peroxisomes, which are organelles involved in many roles including β-oxidation metabolism, and ROS homeostasis (Gonzalez-Riano, 2021; Dalazen, 2014). Dysfunction of these organelles contributes to the aging process and neurodegenerative diseases, including PD (Lin, 2020).

Amantadine is an antiviral and antiparkinson drug, which was exclusively found in the two PD groups (iPD and PD+/LRRK2+), as expected. This trend was consistent for both dust and serum samples (**Figure S26**). Furthermore, levodopa, the most commonly prescribed medication for first-line therapy in PD, was found solely in the household dust of PD participants (iPD and PD+/LRRK2+, **Table S12** for details) (Bloem et al., 2021). Importantly, the intake of amantadine, levodopa, and other dopaminergic drugs (exclusively in the PD groups) may influence the metabolism, and consequently the observed results in the serum samples.

3.4.2. *Serum lipidome*

A total of 313 unique lipids were annotated (Level 2–3) in the serum samples by non-target LC-HRMS analysis (**Table S18**), with 252 in ESI (+) and 61 in ESI (−), see **S2.3** and **Figure S27-28** for details about the filtering and quality control approaches. The most abundant lipid categories in serum included glycerophospholipids, glycerolipids and sphingolipids. Forty-three lipids were statistically significantly different, primarily glycerophospholipids (34 of 43; **Figure S27**). Lipid pathway enrichment analysis, computed with the significant lipids, revealed glycerophospholipid metabolism and sphingolipid metabolism as the most altered pathways (**Table S19**), which is consistent with a previous study performed in serum samples from PD and *LRRK2* carriers (Galper, 2022).

Among the glycerophospholipids, phospathidylcholines (PCs) were significantly decreased in the PD+/LRRK2+ or PD-/LRRK2+ compared to the other groups under study (**Figure S29** and **Table S18**). A significant decrease of PC 14:0_18:2 was observed in the PD+/LRRK2+ compared with the PD-/LRRK2+ and iPD groups. PCs are the most abundant glycerophospholipids in membranes and are involved in the control of inflammation, neuronal differentiation and cholesterol homeostasis (Dahabiyeh et al., 2023; Fernández-Irigoyen et al., 2021). Thus, a decrease in PCs may contribute to the neuroinflammation and disease progression, as previously suggested (Dahabiyeh et al., 2023). In contrast, some lysophosphatidylcholines (LPCs), breakdown products of PCs, were significantly elevated in the PD+/LRRK2+ group, including LPC 18:1 and LPC 16:0 (Fig. 7**A-B**). This is in line with a previous study (Dahabiyeh et al., 2023), suggesting that alterations in LPCs serve as markers of mitochondrial dysfunction, neuroinflammation and oxidative stress processes. Additionally, lysophosphatidylethanolamines (LPEs), LPE 18:0 and LPE O-18:1 (Fig. 7**C-D**), were significantly elevated in the PD+/LRRK2+ group compared with the control group. This in contrast with previous studies performed in plasma (Chang et al., 2022) and serum (Dahabiyeh et al., 2023) of iPD participants, which found decreased levels of LPE with the advance of the disease. Thus, it would be interesting to check further whether this alteration is specific to patients carrying *LRRK2* pathogenic variants.

The quantitative analysis of BAs in serum did not reveal any statistically significant differences (**Table S20**), which is in contrast with recent work on Alzheimer's disease progression in cerebrospinal fluid (CSF) samples (Talavera Andújar, 2024). However, non-significant higher trends of the neuroprotective BAs chenodeoxycholic acid (CDCA), and ursodeoxycholic acid (UDCA) were observed in PD-/LRRK2+ in comparison to the PD groups (**Figure S30A-B**). Higher but non-significant trends of the cytotoxic BA deoxycholic acid (DCA) were also observed in the PD-/LRRK2+ group (**Figure S30C**). Previous research has reported elevated levels of secondary cytotoxic BAs in PD, including DCA and lithocholic acid, correlated with an increase in BA-metabolizing bacteria (Chen and Lin, 2022; Li, 2021). Thus, the non-significant higher trends of BAs found in the PD-/LRRK2+ and iPD

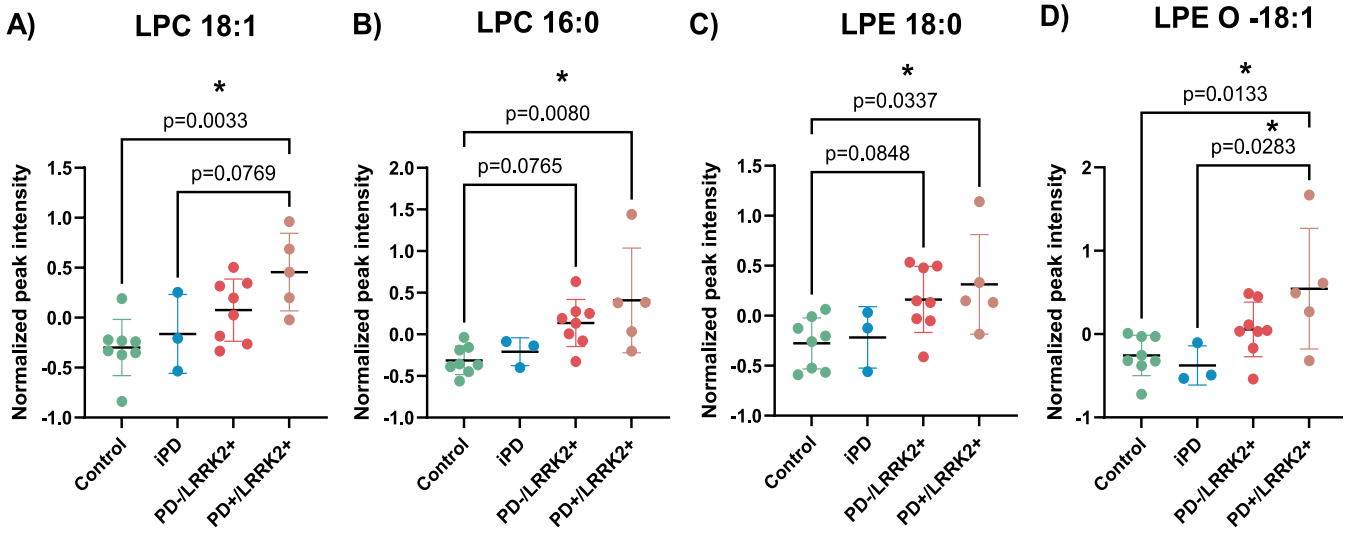

Fig. 7. Bar plots showing the normalized peak intensities across groups of LPC 18:1 **(A),** LPC 16:0 **(B),** LPE 18:0 **(C)**, and LPE 0–18:1 **(D).** p = Tukey's HSD post-hoc p-value. Note that $p < 0.1$ is displayed although only $p < 0.05$ is considered statistically significant here (marked with an "*").

groups may be explained by gut microbiome dysbiosis, as the gut microbiota metabolize the primary BAs to produce secondary BAs such as DCA (Li, 2021). However, this was not investigated further here due to the lack of significance. Since BAs are crucial signaling molecules and key modulators of metabolism and immune homeostasis (Mohanty, 2024), investigating BAs in future studies with larger sample sizes could provide additional insights.

3.5. Effects of BPS on neurons

While the vast majority of studies on BPS so far have focused on its endocrine disrupting effects (Naderi and Kwong, 2020), recent findings have linked this chemical to an elevated risk of neurodegenerative diseases (Xu, 2024). The potential neurotoxic effect of BPS found in the dust samples (Fig. 3**A**) was explored in cultures enriched with dopaminergic neurons generated from a PD individual carrying the *LRRK2* G2019S variant and its isogenic control (IC), as shown in Fig. 8**A**.

Exposure to BPS elicited distinct responses in the IC and PD+/LRRK2+ neurons, particularly at the level of mitochondrial homeostasis. Functional evaluation of mitochondria upon BPS exposure showed that the IC neurons respond by elevating the mitochondrial potential, a response not seen in the PD + cells (Fig. 8**B**). This may be interpreted as a compensatory response of IC neurons to increase ATP production, or conversely, as a result of mild ATP-synthase inhibition, which leads to hyperpolarization of mitochondrial membrane potential due to lower consumption of the mitochondrial proton gradient. Disparate effects of BPS treatment were also observed in the averaged mitochondrial mass, i.e., the volume of mitochondria per cell. Contrarily to the IC, the PD+/LRRK2+ neurons significantly increased their mitochondrial mass (Fig. 8**C**), suggesting that the PD cells accumulate mitochondria due to an impaired mitochondrial clearance mechanism, as previously reported for PD+/LRRK2+ murine models (Singh et al., 2021). Alternatively, the cells may intensify mitochondrial biogenesis to compensate for the BPS-induced insult. Furthermore, BPS negatively impacted (reduced) the organellar size in the PD+/LRRK2+ neurons (Fig. 8**D**), a response commonly seen upon mitochondrial stress, and which is necessary for efficient clearance via mitophagy to occur. Interestingly, BPS had the opposite effect in the IC line at 100 μM, with an increased mitochondrial size detected. Finally, the proposed alterations in mitophagy were supported by the assessment of the normalized colocalization of mitochondria and lysosomes, which suggests that IC neurons more efficiently initiate this clearance process (Fig. 8**E**), and are therefore able to maintain higher mitochondrial fitness. Further experiments, beyond the scope of this current effort, are ongoing to better understand the impact of BPS exposure on neurons.

4. Conclusions and future perspectives

Pilot studies, such as this one, play an important role in health research to develop, assess, and adapt the methods employed, generate hypotheses and provide information for a sample size calculation for a larger trial (Lancaster et al., 2004; Foster, 2013). More specifically, they

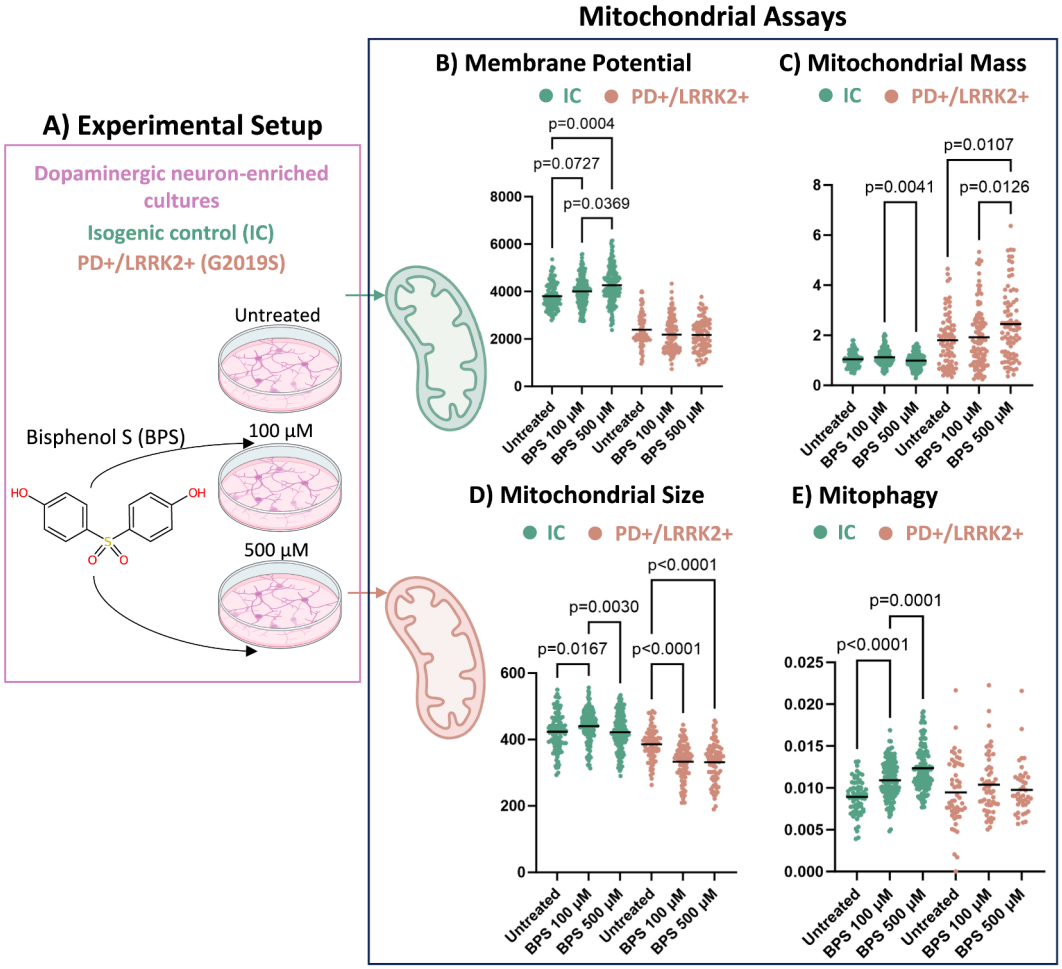

Fig. 8. (**A**) Experimental setup showing the three different conditions for the two groups (PD+/LRRK2+ and isogenic cell lines); untreated, treated with 100 μM of Bisphenol S (BPS) and treated with 500 μM of BPS. (**B**) mitochondrial potential, (**C**) mitochondrial mass, (**D**) mitochondrial size, and E) normalized mitophagy. Kruskal-Wallis test followed by post-hoc Dunn's test (uncorrected) was performed. Dunn's test p-values are displayed in the scatter plots.

can be used to adjust sample sizes, refine sample collection methods, or to determine chemicals of interest for the design of more sensitive analysis methods (e.g., target analysis techniques). Using the results generated in this study, a power analysis was undertaken using the MultiPower method in R (ConesaLab, 2024; Tarazona, 2020) to calculate the optimal sample size for each group comparison integrating both metabolomics/exposomics (1,003 chemicals, **Table S11**), and metagenomics (163 mOTUs, **Table S15**) datasets to help scope future studies. For an average statistical power of 0.8, the estimated minimum sample size for each group in metabolomics/exposomics ranges between 40 and 89, while for metagenomics it is 36–79. The overall optimal sample size would thus be 273 (**Table S21** for details), and the minimum sample size required per group comparison and omic dataset (metabolomics and metagenomics) is shown in **Figure S31**, which is a challenge for specialized cohorts such as this one.

In this pilot study, several significant differences were found in the indoor dust chemical and microbial composition across study groups. Although previous studies have indicated that household dust acts a reservoir of several chemicals and microbial taxa that may pose a risk to human health (Shan et al., 2019; Rostkowski, 2019; Fuentes-Ferragud et al., 2023), to our knowledge, the present study represents one of the early substantial efforts to investigate the dust metabolome/exposome and microbiome in the context of PD, and more specifically in PD associated with the penetrance of *LRRK2* pathogenic variants. BPS, PFAS, and BThs showed significantly higher levels in the PD+/LRRK2+ group compared with the PD-/LRRK2+ and should be investigated further (with a larger sample size) to determine whether they could be potential modifiers of *LRRK2* penetrance associated with PD. Moreover, several taxa and KOs were significantly different between groups, with various species (e.g., *Clavibacter michiganensis* and *Marmoricola* sp. *Leaf446*) displaying significantly lower abundances in the PD-/LRRK2+ group compared to the iPD group (**Figure S20**). In line with previous reports based on the nasal microbiota from PD patients (Pereira et al., 2017), it is worth investigating whether the household environment could be responsible for some of the observations in the host microbiome in future studies. Since oral ingestion of dust is a potential source of exposure to environmental contaminants, especially concerning for infants/toddlers, the connection between dust and the oral-gut axis (Kunath et al., 2024) could be of interest for future investigations. Differences in the serum lipidome and metabolome were observed, partially matching previously published works. However, most of the chemicals found in dust, which may be potential risks for human health, were not found in the serum samples. This may be because exogenous chemicals are present at trace levels in biological samples compared with endogenous chemicals (David, 2021).

This study has provided valuable insights for both collecting additional patient information as well as designing future sample collection procedures that will enable better consideration of relevant lifestyle factors in the next investigations. While the small sample size is the main limitation of our study, monogenic PD only occurs in about 5 % of patients and this study specifically focused on an even smaller subset of affected and unaffected carriers of pathogenic variants in the *LRRK2* gene, with the specific aim to explore the contribution of environmental factors to penetrance. The statistically relevant number of dust samples was only obtained due to access to the unique LIPAD study cohort (Usnich et al., 2021), which enabled pursuit of this challenging research objective. However, the design of the LIPAD study also restricted the sample matching in this study and the discrepancy in the average age of the PD-/LRRK2+ group and the PD+/LRRK2+ may have confounded the results. Since the PD-/LRRK2+ group was on average 10 years younger than the PD+/LRRK2+ group, some of the currently asymptomatic individuals with *LRRK2* pathogenic variants may still develop PD later in life. Other confounding factors that may have influenced the observed differences in both dust and serum include diet, smoking and the use of medication.

While this current effort involved samples primarily from Germany (36), it also included a limited number of samples from Turkey (5). Since multivariate analysis revealed no clear geographic differences (**Figure S9**), further exploration of environmental factors across geographic regions was not further pursued. As the LIPAD cohort develops and more samples become available, it will be easier to match the demographic data of the samples and to form more geographically coherent sample sets, which will ease the data interpretation. Furthermore, all the samples were collected from respective households at a single point in time as part of a cross-sectional study, with individuals already diagnosed, which could lead to a risk of reverse causation when interpreting the results. Future longitudinal studies that collect samples across different time points are essential to validate the results of this research.

Household dust samples can be heterogenous and highly variable, both intra-day and inter-day. The collection of dust samples via vacuum cleaner bags can add further to this variability. While improving dust sample collection is a subject under discussion, the experience obtained here shows that the advantages of a simple dust sample collection protocol currently outweigh the disadvantages. While this approach may lead to more variability due to the different vacuum cleaner systems used by the participants, it allows for an easy enlargement of the cohort size. More advanced collection systems require training of both nursing staff and participants and would rapidly become financially unfeasible within the context of a cohort study like LIPAD that was designed to carry out a clinical trial.

Finally, this study demonstrated that BPS, a compound found in the household dust samples with statistically significant differences between groups, negatively affected mitochondrial function in PD+/LRRK2+ and isogenic control neurons, providing avenues for further investigation. This underscores the importance of exposome studies in prioritizing chemicals for further exploration with patient-derived *in vitro* models. Of note, the investigated patient midbrain neurons harbored the G2019S change in *LRRK2*, which is the most frequent PD-linked pathogenic variant, and the most abundant variant in the cohort investigated here. Hence, this pilot study connected, for the first time, all of exposomics, in vivo and in vitro analyses to obtain unique insights into how environmental factors may modulate molecular mechanisms that define the penetrance of PD gene pathogenic variants.

Ethics declarations.

The studies involving human participants were reviewed and approved by the Ethics Board of the University of Lübeck (Germany) "ProtectMove (FOR 2488)" and the Luxembourg Comité National d'Ethique de Recherche of Luxembourg.

CRediT authorship contribution statement

Begoña Talavera Andújar: Writing – review & editing, Writing – original draft, Visualization, Methodology, Investigation, Formal analysis, Data curation, Conceptualization. **Sandro L. Pereira:** Writing – review & editing, Supervision, Investigation, Formal analysis, Data curation. **Susheel Bhanu Busi:** Writing – review & editing, Supervision, Investigation, Formal analysis, Data curation. **Tatiana Usnich:** Writing – review & editing, Resources, Investigation. **Max Borsche:** Writing – review & editing, Resources. **Sibel Ertan:** Writing – review & editing, Supervision, Resources, Investigation. **Peter Bauer:** Writing – review & editing, Resources. **Arndt Rolfs:** Writing – review & editing, Resources. **Soraya Hezzaz:** Methodology, Investigation. **Jenny Ghelfi:** Methodology, Investigation. **Norbert Brüggemann:** Writing – review & editing, Resources. **Paul Antony:** Writing – review & editing, Supervision, Resources, Methodology, Investigation, Funding acquisition, Conceptualization. **Paul Wilmes:** Writing – review & editing, Supervision, Resources, Methodology, Investigation, Funding acquisition, Conceptualization. **Christine Klein:** Writing – review & editing, Supervision, Resources, Funding acquisition, Conceptualization. **Anne Grünewald:** Writing – review & editing, Supervision, Resources, Funding acquisition, Conceptualization. **Emma L. Schymanski:** Writing – review & editing,

Writing – original draft, Supervision, Resources, Methodology, Investigation, Funding acquisition, Conceptualization.

Declaration of competing interest

The authors declare that they have no known competing financial interests or personal relationships that could have appeared to influence the work reported in this paper.

Acknowledgements

We thank the Metabolomics Platform of the LCSB for their support with the LC-HRMS analysis. Floriane Gavotto is acknowledged for performing the target LC-MS analysis of the bile acids and the help during data processing with TraceFinder. Rashi Halder and all the sequencing platform of the LCSB is acknowledged for performing the sequencing experiment. The Bioimaging Platform of the LCSB is acknowledged for the support with the imaging analysis of the cell-based experiments. Meike Kasten, MD and Eva-Juliane Vollstedt, MD from the Institute of Neurogenetics, University of Luebeck are acknowledged for their contributions to the design and development of the LIPAD study. Prof. Dr. Özgür Öztop Çakmak and Prof. Dr. Ayşe Nazlı Başak from the Department of Neurology, Koc University, Turkey, are acknowledged for their contributions towards the Turkish LRRK2 samples. We thank Dr. Leonid Zaslavsky, Dr. Evan Bolton, and Dr. Tiejun Cheng from the PubChem Team for the help preparing the LRRK2 suspect list of chemicals. Dr. Gianfranco Frigerio is acknowledged for his inputs during the dust sample preparation and data processing. We acknowledge Veronica Codoni for her assistance with the power analysis calculation and its interpretation. The computational analyses presented in this paper were carried out using the HPC facilities at the University of Luxembourg (Homepage | HPC @ Uni.lu, 2024; Varrette et al., 2014).

Funding

BTA is part of the "Microbiomes in One Health" PhD training program, which is supported by the PRIDE doctoral research funding scheme (PRIDE/11823097) of the Luxembourg National Research Fund (FNR). ELS acknowledges funding support from the Luxembourg National Research Fund (FNR) for project A18/BM/12341006. AG received funds from the FNR within the framework of the INTER grants "ProtectMove I and II" (FNR11250962 and INTER/DFG/19/14429377) and the ATTRACT career development grant "Model-IPD" (FNR9631103). The LIPAD study has been supported by institutional funds (Institute of Neurogenetics, University of Lübeck), and was partly supported by Centogene GmbH. Moreover, this study was supported by the German Research Foundation (DFG, ProtectMove FOR2488 to CK, NB, and AG).

Appendix A. Supplementary material

Supplementary data to this article can be found online at https://doi.org/10.1016/j.envint.2024.109151.

Data availability

The code functions and files associated with this manuscript are provided in the ECI GitLab repository: https://gitlab.com/uniluxembourg/lcsb/eci/pd-lrrk2.

References

"DNeasy PowerLyzer PowerSoil Kit." Accessed: Mar. 13, 2024. [Online]. Available: https://www.qiagen.com/us/products/discovery-and-translational-research/dna-rna-purification/dna-purification/microbial-dna/dneasy-powerlyzer-powersoil-kit.

"Homepage | HPC @ Uni.lu." Accessed: Mar. 26, 2024. [Online]. Available: https://hpc.uni.lu/.

"KEGGREST," Bioconductor. Accessed: Mar. 12, 2024. [Online]. Available: http://bioconductor.org/packages/KEGGREST/.

"LIPEA | What is LIPEA?" Accessed: Mar. 05, 2024. [Online]. Available: https://hyperlipea.org/about/what.

"NORMAN Network | NORMAN." Accessed: Mar. 07, 2024. [Online]. Available: https://www.norman-network.com/?q=node/4.

"PubChem Classification Browser." Accessed: May 19, 2024. [Online]. Available: https://pubchem.ncbi.nlm.nih.gov/classification/#hid=72.

"PubChem Classification Browser." Accessed: May 20, 2024. [Online]. Available: https://pubchem.ncbi.nlm.nih.gov/classification/#hid=101.

N. Alygizakis and J. Slobodnik, "S32 | REACH2017 | >68,600 REACH Chemicals." Zenodo. 20, 2018. doi: 10.5281/zenodo.2653021.

An, H., Yu, H., Wei, Y., Liu, F., Ye, J., 2021. Disrupted metabolic pathways and potential human diseases induced by bisphenol S. Environ. Toxicol. Pharmacol. 88, 103751. https://doi.org/10.1016/j.etap.2021.103751.

K. S. Andersen, *KasperSkytte/ampvis2*. (Jan. 16, 2024). R. Accessed: Feb. 19, 2024. [Online]. Available: https://github.com/KasperSkytte/ampvis2.

S. Andres and V. Dulio, "S109 | PARCEDC | List of 7074 potential endocrine disrupting compounds (EDCs) by PARC T4.2." Zenodo. 08, 2024. doi: 10.5281/zenodo.10944199.

Begoña Talavera Andújar, "uniluxembourg / LCSB / Environmental Cheminformatics / PD-LRRK2 · GitLab," GitLab. Accessed: Jul. 18, 2024. [Online]. Available: https://gitlab.com/uniluxembourg/lcsb/eci/pd-lrrk2.

N. Baker, E. Schymanski, and A. Williams, "S37 | LITMINEDNEURO | Neurotoxicants from literature mining PubMed." Zenodo. 10, 2019. doi: 10.5281/zenodo.3242298.

Baumuratov, A.S., et al., 2016. Enteric neurons from Parkinson's disease patients display ex vivo aberrations in mitochondrial structure. Sci. Rep. 6 (1), 33117. https://doi.org/10.1038/srep33117.

Bjørklund, G., Dadar, M., Chirumbolo, S., Aaseth, J., 2020. The Role of Xenobiotics and Trace Metals in Parkinson's Disease. Mol. Neurobiol. 57 (3), 1405–1417. https://doi.org/10.1007/s12035-019-01832-1.

Bloem, B.R., Okun, M.S., Klein, C., 2021. Parkinson's disease. Lancet 397 (10291), 2284–2303. https://doi.org/10.1016/S0140-6736(21)00218-X.

Boktor, J.C., et al., 2023. Integrated Multi-Cohort Analysis of the Parkinson's Disease Gut Metagenome. Mov. Disord. 38 (3), 399–409. https://doi.org/10.1002/mds.29300.

Bose, A., Beal, M.F., 2016. Mitochondrial dysfunction in Parkinson's disease. J. Neurochem. 139 (S1), 216–231. https://doi.org/10.1111/jnc.13731.

Broadhurst, D., et al., 2018. Guidelines and considerations for the use of system suitability and quality control samples in mass spectrometry assays applied in untargeted clinical metabolomic studies. Metabolomics 14 (6), 72. https://doi.org/10.1007/s11306-018-1367-3.

Cajka, T., Smilowitz, J.T., Fiehn, O., 2017. Validating Quantitative Untargeted Lipidomics Across Nine Liquid Chromatography–High-Resolution Mass Spectrometry Platforms. Anal. Chem. 89 (22), 12360–12368. https://doi.org/10.1021/acs.analchem.7b03404.

Cao, S., et al., 2023. Prenatal exposure to benzotriazoles and benzothiazoles and child neurodevelopment: A longitudinal study. Sci. Total Environ. 865, 161188. https://doi.org/10.1016/j.scitotenv.2022.161188.

Chambers, M.C., et al., 2012. A cross-platform toolkit for mass spectrometry and proteomics. Nat. Biotechnol. 30 (10), 918–920. https://doi.org/10.1038/nbt.2377.

K.-H. Chang, M.-L. Cheng, H.-Y. Tang, C.-Y. Huang, H.-C. Wu, and C.-M. Chen, "Alterations of Sphingolipid and Phospholipid Pathways and Ornithine Level in the Plasma as Biomarkers of Parkinson's Disease," *Cells*, vol. 11, no. 3, Art. no. 3. 2022, doi: 10.3390/cells11030395.

Chen, S.-J., Lin, C.-H., 2022. Gut microenvironmental changes as a potential trigger in Parkinson's disease through the gut–brain axis. J. Biomed. Sci. 29 (1), 54. https://doi.org/10.1186/s12929-022-00839-6.

Chong, J., Liu, P., Zhou, G., Xia, J., 2020. Using MicrobiomeAnalyst for comprehensive statistical, functional, and meta-analysis of microbiome data. Nat. Protoc. 15 (3), 799–821. https://doi.org/10.1038/s41596-019-0264-1.

ConesaLab/MultiPower. (Mar. 12, 2024). R. ConesaLab - Genomics of gene expression. Accessed: Mar. 27, 2024. [Online]. Available: https://github.com/ConesaLab/MultiPower.

Cousins, I.T., et al., 2020. The high persistence of PFAS is sufficient for their management as a chemical class. Environ. Sci. Process. Impacts 22 (12), 2307–2312. https://doi.org/10.1039/D0EM00355G.

L. A. Dahabiyeh, R. M. Nimer, M. Rashed, J. D. Wells, and O. Fiehn, "Serum-Based Lipid Panels for Diagnosis of Idiopathic Parkinson's Disease," *Metabolites*, vol. 13, no. 9, Art. no. 9. 2023, doi: 10.3390/metabo13090990.

Dalazen, G.R., et al., 2014. Pipecolic acid induces oxidative stress in vitro in cerebral cortex of young rats and the protective role of lipoic acid. Metab. Brain Dis. 29 (1), 175–183. https://doi.org/10.1007/s11011-013-9466-3.

David, A., et al., 2021. Towards a comprehensive characterisation of the human internal chemical exposome: Challenges and perspectives. Environ. Int. 156, 106630. https://doi.org/10.1016/j.envint.2021.106630.

De Wever, H., Verachtert, H., Besse, P., 2001. Microbial transformations of 2-substituted benzothiazoles. Appl. Microbiol. Biotechnol. 57 (5–6), 620–625. https://doi.org/10.1007/s00253-001-0842-2.

N. Dodder and K. Mullen, *OrgMassSpecR: Organic Mass Spectrometry*. (Aug. 13, 2017). Accessed: Jan. 29, 2024. [Online]. Available: https://cran.r-project.org/web/packages/OrgMassSpecR/index.html.

Dubocq, F., Kärrman, A., Gustavsson, J., Wang, T., 2021. Comprehensive chemical characterization of indoor dust by target, suspect screening and nontarget analysis using LC-HRMS and GC-HRMS. Environ. Pollut. 276, 116701. https://doi.org/10.1016/j.envpol.2021.116701.

Eichenlaub, R., Gartemann, K.-H., 2011. The Clavibacter michiganensis Subspecies: Molecular Investigation of Gram-Positive Bacterial Plant Pathogens. Annu. Rev. Phytopathol. 49 (1), 445–464. https://doi.org/10.1146/annurev-phyto-072910-095258.

J. Fernández-Irigoyen, P. Cartas-Cejudo, M. Iruarrizaga-Lejarreta, and E. Santamaría, "Alteration in the Cerebrospinal Fluid Lipidome in Parkinson's Disease: A Post-Mortem Pilot Study," *Biomedicines*, vol. 9, no. 5, Art. no. 5 2021, doi: 10.3390/biomedicines9050491.

Foster, R.L., 2013. What a pilot study is and what it is not. J. Spec. Pediatr. Nurs. 18 (1), 1–2. https://doi.org/10.1111/jspn.12015.

Fuentes-Ferragud, E., Miralles, P., López, A., Ibáñez, M., Coscollà, C., 2023. Non-target screening and human risk assessment for adult and child populations of semi-volatile organic compounds in residential indoor dust in Spain. Chemosphere 340, 139879. https://doi.org/10.1016/j.chemosphere.2023.139879.

M. Fujimaki *et al.*, "Serum caffeine and metabolites are reliable biomarkers of early Parkinson disease," *Neurology*, vol. 90, no. 5. 2018, doi: 10.1212/WNL.0000000000004888.

Galper, J., et al., 2022. "Lipid pathway dysfunction is prevalent in patients with Parkinson's disease", *Brain.* J. Neurol. p. awac176. https://doi.org/10.1093/brain/awac176.

Gonzalez-Riano, C., et al., 2021. Prognostic biomarkers of Parkinson's disease in the Spanish EPIC cohort: a multiplatform metabolomics approach. Npj Park. Dis. 7 (1), 1–12. https://doi.org/10.1038/s41531-021-00216-4.

Graham, S.F., et al., 2018. Metabolomic Profiling of Bile Acids in an Experimental Model of Prodromal Parkinson's Disease. Metabolites 8 (4), 71. https://doi.org/10.3390/metabo8040071.

K. Groh and E. Schymanski, "S49 | CPPDBLISTB | Database of Chemicals possibly (List B) associated with Plastic Packaging (CPPdb)." Zenodo. 06, 2019. doi: 10.5281/ZENODO.2658152.

Gu, J., Guo, L., Chen, C., Ji, G., Wang, L., 2024. Neurobehavioral toxic effects and mechanisms of 2-aminobenzothiazole exposure on zebrafish. Sci. Total Environ. 913, 169495. https://doi.org/10.1016/j.scitotenv.2023.169495.

Gyimah, E., et al., 2021. Developmental neurotoxicity of low concentrations of bisphenol A and S exposure in zebrafish. Chemosphere 262, 128045. https://doi.org/10.1016/j.chemosphere.2020.128045.

P. Haglund and P. Rostkowski, "S35 | INDOORCT16 | Indoor Environment Substances from 2016 Collaborative Trial," Feb. 2019, doi: 10.5281/zenodo.6848859.

Healy, D.G., et al., 2008. Phenotype, genotype, and worldwide genetic penetrance of *LRRK2*-associated Parkinson's disease: a case-control study. Lancet Neurol. 7 (7), 583–590. https://doi.org/10.1016/S1474-4422(08)70117-0.

R. Helmus, T. L. ter Laak, A. P. van Wezel, P. de Voogt, and E. L. Schymanski, *patRoon: open source software platform for environmental mass spectrometry based non-target screening.* (Jan. 2021). R. doi: 10.1186/s13321-020-00477-w.

Helmus, R., van de Velde, B., Brunner, A.M., ter Laak, T.L., van Wezel, A.P., Schymanski, E.L., 2022. patRoon 2.0: Improved non-target analysis workflows including automated transformation product screening. J. Open Source Softw. 7 (71), 4029. https://doi.org/10.21105/joss.04029.

Hentati, F., Trinh, J., Thompson, C., Nosova, E., Farrer, M.J., Aasly, J.O., 2014. LRRK2 parkinsonism in Tunisia and Norway: A comparative analysis of disease penetrance. Neurology 83 (6), 568–569. https://doi.org/10.1212/WNL.0000000000000675.

Höglinger, G.U., et al., 2024. A biological classification of Parkinson's disease: the SynNeurGe research diagnostic criteria. Lancet Neurol. 23 (2), 191–204. https://doi.org/10.1016/S1474-4422(23)00404-0.

Hollender, J., et al., 2023. NORMAN guidance on suspect and non-target screening in environmental monitoring. Environ. Sci. Eur. 35 (1), 75. https://doi.org/10.1186/s12302-023-00779-4.

Hornung, M.W., et al., 2015. In Vitro, Ex Vivo, and In Vivo Determination of Thyroid Hormone Modulating Activity of Benzothiazoles. Toxicol. Sci. 146 (2), 254–264. https://doi.org/10.1093/toxsci/kfv090.

Hu, C., Huang, Z., Sun, B., Liu, M., Tang, L., Chen, L., 2022. Metabolomic profiles in zebrafish larvae following probiotic and perfluorobutanesulfonate coexposure. Environ. Res. 204, 112380. https://doi.org/10.1016/j.envres.2021.112380.

Kathage, J., Castañera, P., Alonso-Prados, J.L., Gómez-Barbero, M., Rodríguez-Cerezo, E., 2018. The impact of restrictions on neonicotinoid and fipronil insecticides on pest management in maize, oilseed rape and sunflower in eight European Union regions. Pest Manag. Sci. 74 (1), 88–99. https://doi.org/10.1002/ps.4715.

Kim, S., et al., 2023. PubChem 2023 update. Nucleic Acids Res. 51 (D1), D1373–D1380. https://doi.org/10.1093/nar/gkac956.

T. Kind, K.-H. Liu, D. Y. Lee, B. DeFelice, J. K. Meissen, and O. Fiehn, "LipidBlast in silico tandem mass spectrometry database for lipid identification," *Nat. Methods*, vol. 10, no. 8, Art. no. 8. 2013, doi: 10.1038/nmeth.2551.

Kleespies, R.G., Federici, B.A., Leclerque, A., 2014. Ultrastructural characterization and multilocus sequence analysis (MLSA) of '*Candidatus* Rickettsiella isopodorum', a new lineage of intracellular bacteria infecting woodlice (Crustacea: Isopoda). Syst. Appl. Microbiol. 37 (5), 351–359. https://doi.org/10.1016/j.syapm.2014.04.001.

Koelmel, J.P., et al., 2017. LipidMatch: an automated workflow for rule-based lipid identification using untargeted high-resolution tandem mass spectrometry data. BMC Bioinf. 18 (1), 331. https://doi.org/10.1186/s12859-017-1744-3.

Kunath, B.J., De Rudder, C., Laczny, C.C., Letellier, E., Wilmes, P., 2024. The oral–gut microbiome axis in health and disease. Nat. Rev. Microbiol. 1–15. https://doi.org/10.1038/s41579-024-01075-5.

Lancaster, G.A., Dodd, S., Williamson, P.R., 2004. Design and analysis of pilot studies: recommendations for good practice. J. Eval. Clin. Pract. 10 (2), 307–312. https://doi.org/10.1111/j.2002.384.doc.x.

Lange, M., Fedorova, M., 2020. Evaluation of lipid quantification accuracy using HILIC and RPLC MS on the example of NIST® SRM® 1950 metabolites in human plasma. Anal. Bioanal. Chem. 412 (15), 3573–3584. https://doi.org/10.1007/s00216-020-02576-x.

Li, P., et al., 2021. Gut Microbiota Dysbiosis Is Associated with Elevated Bile Acids in Parkinson's Disease. Metabolites 11 (1), 29. https://doi.org/10.3390/metabo11010029.

Liao, C., Kim, U.-J., Kannan, K., 2018. A Review of Environmental Occurrence, Fate, Exposure, and Toxicity of Benzothiazoles. Environ. Sci. Technol. 52 (9), 5007–5026. https://doi.org/10.1021/acs.est.7b05493.

Lilienblum, W., et al., 2008. Alternative methods to safety studies in experimental animals: role in the risk assessment of chemicals under the new European Chemicals Legislation (REACH). Arch. Toxicol. 82 (4), 211–236. https://doi.org/10.1007/s00204-008-0279-9.

Lim, S.-Y., Klein, C., 2024. Parkinson's Disease is Predominantly a Genetic Disease. J. Park. Dis. 14 (3), 467–482. https://doi.org/10.3233/JPD-230376.

Lin, T.-K., et al., 2020. When Friendship Turns Sour: Effective Communication Between Mitochondria and Intracellular Organelles in Parkinson's Disease. Front. Cell Dev. Biol. 8, 607392. https://doi.org/10.3389/fcell.2020.607392.

Loh, J.S., et al., 2024. Microbiota–gut–brain axis and its therapeutic applications in neurodegenerative diseases. Signal Transduct. Target. Ther. 9 (1), 1–53. https://doi.org/10.1038/s41392-024-01743-1.

Lu, Y., Zhou, G., Ewald, J., Pang, Z., Shiri, T., Xia, J., 2023. MicrobiomeAnalyst 2.0: comprehensive statistical, functional and integrative analysis of microbiome data. Nucleic Acids Res. 51 (W1), W310–W318. https://doi.org/10.1093/nar/gkad407.

Lubomski, M., Tan, A.H., Lim, S.-Y., Holmes, A.J., Davis, R.L., Sue, C.M., 2020. Parkinson's disease and the gastrointestinal microbiome. J. Neurol. 267 (9), 2507–2523. https://doi.org/10.1007/s00415-019-09320-1.

Lüth, T., et al., 2023. Interaction of Mitochondrial Polygenic Score and Lifestyle Factors in LRRK2 p.Gly2019Ser Parkinsonism. Mov. Disord. off. J. Mov. Disord. Soc. 38 (10), 1837–1849. https://doi.org/10.1002/mds.29563.

Y. Ma *et al.*, "Nocardioides: 'Specialists' for Hard-to-Degrade Pollutants in the Environment," *Molecules*, vol. 28, no. 21, Art. no. 21. 2023, doi: 10.3390/molecules28217433.

Matsuda, Y., Higashino, K., Adachi, K., Amuro, Y., Hada, T., 1995. Production of pipecolic acid from intestinal bacteria: Plasma levels of pipecolic acid in patients with liver cirrhosis decreased after oral kanamycin administration. Int. Hepatol. Commun. 4 (1), 26–34. https://doi.org/10.1016/0928-4346(95)00210-A.

J. Mayfield, "CDK Depict Web Interface." 2023. Accessed: Mar. 09, 2023. [Online]. Available: https://www.simolecule.com/cdkdepict/depict.html.

Miller, M., Cook, L., Verbrugge, J., Hodges, P.D., Head, K.J., Nance, M.A., 2024. Delivering Genetic Test Results for Parkinson Disease. Neurol. Clin. Pract. 14 (2), e200282.

Min, E.K., et al., 2023. Integrative multi-omics reveals analogous developmental neurotoxicity mechanisms between perfluorobutanesulfonic acid and perfluorooctanesulfonic acid in zebrafish. J. Hazard. Mater. 457, 131714. https://doi.org/10.1016/j.jhazmat.2023.131714.

Mohanty, I., et al., 2024. The changing metabolic landscape of bile acids – keys to metabolism and immune regulation. Nat. Rev. Gastroenterol. Hepatol. 21 (7), 493–516. https://doi.org/10.1038/s41575-024-00914-3.

Moschet, C., Anumol, T., Lew, B.M., Bennett, D.H., Young, T.M., 2018. Household dust as a repository of chemical accumulation: New insights from a comprehensive high-resolution mass spectrometry study. Environ. Sci. Technol. 52 (5), 2878–2887. https://doi.org/10.1021/acs.est.7b05767.

Naderi, M., Kwong, R.W.M., 2020. A comprehensive review of the neurobehavioral effects of bisphenol S and the mechanisms of action: New insights from in vitro and in vivo models. Environ. Int. 145, 106078. https://doi.org/10.1016/j.envint.2020.106078.

Narayanasamy, S., et al., 2016. IMP: a pipeline for reproducible reference-independent integrated metagenomic and metatranscriptomic analyses. Genome Biol. 17 (1), 260. https://doi.org/10.1186/s13059-016-1116-8.

Shaman Narayanasamy, Yohan Jarosz, and Anna Heintz-Buschart, "IMP / IMP3 · GitLab," GitLab. Accessed: Mar. 26, 2024. [Online]. Available: https://gitlab.lcsb.uni.lu/IMP/imp3.

Nazar, N., et al., 2024. Untargeted metabolomics reveals potential health risks associated with chronic exposure to environmentally relevant concentrations of 2-Phenylphenol. Sci. Total Environ. 912, 169172. https://doi.org/10.1016/j.scitotenv.2023.169172.

Nickels, S.L., et al., 2019. Impaired serine metabolism complements LRRK2-G2019S pathogenicity in PD patients. Parkinsonism Relat. Disord. 67, 48–55. https://doi.org/10.1016/j.parkreldis.2019.09.018.

Nielsen, N.J., Christensen, P., Poulsen, K.G., Christensen, J.H., 2023. Investigation of micropollutants in household waste fractions processed by anaerobic digestion: target analysis, suspect- and non-target screening. Environ. Sci. Pollut. Res. 30 (16), 48491–48507. https://doi.org/10.1007/s11356-023-25692-4.

Nontargeted Comprehensive Two-Dimensional Gas Chromatography/Time-of-Flight Mass Spectrometry Method and Software for Inventorying Persistent and Bioaccumulative Contaminants in Marine Environments. Environ. Sci. Technol. 2012, 46, 15, 8001–8008. https://doi.org/10.1021/es301139q.

Palacios Colón, L., Rascón, A.J., Hejji, L., Azzouz, A., Ballesteros, E., 2021. Validation and Use of an Accurate, Sensitive Method for Sample Preparation and Gas Chromatography-Mass Spectrometry Determination of Different Endocrine-Disrupting Chemicals in Dairy Products. Foods 10 (5), 1040. https://doi.org/10.3390/foods10051040.

Pang, Z., et al., 2024. MetaboAnalyst 6.0: towards a unified platform for metabolomics data processing, analysis and interpretation. Nucleic Acids Res. p. gkae253. https://doi.org/10.1093/nar/gkae253.

Pereira, P.A.B., Aho, V.T.E., Paulin, L., Pekkonen, E., Auvinen, P., Scheperjans, F., 2017. Oral and nasal microbiota in Parkinson's disease. Parkinsonism Relat. Disord. 38, 61–67. https://doi.org/10.1016/j.parkreldis.2017.02.026.

Qian, Y., et al., 2018. Alteration of the fecal microbiota in Chinese patients with Parkinson's disease. Brain. Behav. Immun. 70, 194–202. https://doi.org/10.1016/j.bbi.2018.02.016.

Qing, X., Walter, J., Jarazo, J., Arias-Fuenzalida, J., Hillje, A.-L., Schwamborn, J.C., 2017. CRISPR/Cas9 and piggyBac-mediated footprint-free LRRK2-G2019S knock-in reveals neuronal complexity phenotypes and α-Synuclein modulation in dopaminergic neurons. Stem Cell Res. 24, 44–50. https://doi.org/10.1016/j.scr.2017.08.013.

Reinhardt, P., et al., 2013. Derivation and Expansion Using Only Small Molecules of Human Neural Progenitors for Neurodegenerative Disease Modeling. PLoS One 8 (3), e59252.

Reinhardt, P., et al., 2013. Genetic Correction of a LRRK2 Mutation in Human iPSCs Links Parkinsonian Neurodegeneration to ERK-Dependent Changes in Gene Expression. Cell Stem Cell 12 (3), 354–367. https://doi.org/10.1016/j.stem.2013.01.008.

Rohart, F., Gautier, B., Singh, A., Cao, K.-A.-L., 2017. mixOmics: An R package for 'omics feature selection and multiple data integration. PLOS Comput. Biol. 13 (11), e1005752.

Romano, S., Savva, G.M., Bedarf, J.R., Charles, I.G., Hildebrand, F., Narbad, A., 2021. Meta-analysis of the Parkinson's disease gut microbiome suggests alterations linked to intestinal inflammation. Npj Park. Dis. 7 (1), 27. https://doi.org/10.1038/s41531-021-00156-z.

Rostkowski, P., et al., 2019. The strength in numbers: comprehensive characterization of house dust using complementary mass spectrometric techniques. Anal. Bioanal. Chem. 411 (10), 1957–1977. https://doi.org/10.1007/s00216-019-01615-6.

Sakowski, S.A., Koubek, E.J., Chen, K.S., Goutman, S.A., Feldman, E.L., 2024. Role of the Exposome in Neurodegenerative Disease: Recent Insights and Future Directions. Ann. Neurol. 95 (4), 635–652. https://doi.org/10.1002/ana.26897.

Salis, S., et al., 2017. Occurrence of imidacloprid, carbendazim, and other biocides in Italian house dust: Potential relevance for intakes in children and pets. J. Environ. Sci. Health Part B 52 (9), 699–709. https://doi.org/10.1080/03601234.2017.1331675.

Schirmer, E., Schuster, S., Machnik, P., 2021. Bisphenols exert detrimental effects on neuronal signaling in mature vertebrate brains. Commun. Biol. 4 (1), 1–9. https://doi.org/10.1038/s42003-021-01966-w.

Schneider, S.A., Alcalay, R.N., 2017. Neuropathology of genetic synucleinopathies with parkinsonism: Review of the literature. Mov. Disord. 32 (11), 1504–1523. https://doi.org/10.1002/mds.27193.

Schwarzenbach, R.P., et al., 2006. The Challenge of Micropollutants in Aquatic Systems. Science 313 (5790), 1072–1077. https://doi.org/10.1126/science.1127291.

Seemann, T., 2014. Prokka: rapid prokaryotic genome annotation. Bioinformatics 30 (14), 2068–2069. https://doi.org/10.1093/bioinformatics/btu153.

Shan, Y., et al., 2020. Modern urbanization has reshaped the bacterial microbiome profiles of house dust in domestic environments. World Allergy Organ. J. 13 (8), 100452. https://doi.org/10.1016/j.waojou.2020.100452.

Shan, Y., Wu, W., Fan, W., Haahtela, T., Zhang, G., 2019. House dust microbiome and human health risks. Int. Microbiol. 22 (3), 297–304. https://doi.org/10.1007/s10123-019-00057-5.

Siderowf, A., et al., 2023. Assessment of heterogeneity among participants in the Parkinson's Progression Markers Initiative cohort using α-synuclein seed amplification: a cross-sectional study. Lancet Neurol. 22 (5), 407–417. https://doi.org/10.1016/S1474-4422(23)00109-6.

Singh, F., Prescott, A.R., Rosewell, P., Ball, G., Reith, A.D., Ganley, I.G., 2021. "pharmacological Rescue of Impaired Mitophagy in Parkinson's Disease-Related LRRK2 G2019S Knock-in Mice", *eLife* vol. 10, e67604.

Skrahina, V., et al., 2021. The Rostock International Parkinson's Disease (ROPAD) Study: Protocol and Initial Findings. Mov. Disord. off. J. Mov. Disord. Soc. 36 (4), 1005–1010. https://doi.org/10.1002/mds.28416.

Steinmetz, J.D., et al., 2024. Global, regional, and national burden of disorders affecting the nervous system, 1990–2021: a systematic analysis for the Global Burden of Disease Study 2021. Lancet Neurol. 23 (4), 344–381. https://doi.org/10.1016/S1474-4422(24)00038-3.

Subramaniam, S.R., Chesselet, M.-F., 2013. Mitochondrial dysfunction and oxidative stress in Parkinson's disease. Prog. Neurobiol. 106–107, 17–32. https://doi.org/10.1016/j.pneurobio.2013.04.004.

Takeshige-Amano, H., et al., 2020. Shared Metabolic Profile of Caffeine in Parkinsonian Disorders. Mov. Disord. 35 (8), 1438–1447. https://doi.org/10.1002/mds.28068.

Talavera Andújar, B., et al., 2022. Studying the Parkinson's disease metabolome and exposome in biological samples through different analytical and cheminformatics approaches: a pilot study. Anal. Bioanal. Chem. https://doi.org/10.1007/s00216-022-04207-z.

Talavera Andújar, B., et al., 2024. Can Small Molecules Provide Clues on Disease Progression in Cerebrospinal Fluid from Mild Cognitive Impairment and Alzheimer's Disease Patients? Environ. Sci. Technol. https://doi.org/10.1021/acs.est.3c10490.

Tarazona, S., et al., 2020. Harmonization of quality metrics and power calculation in multi-omic studies. Nat. Commun. 11 (1), 3092. https://doi.org/10.1038/s41467-020-16937-8.

Testa, C., Salis, S., Rubattu, N., Roncada, P., Miniero, R., Brambilla, G., 2019. Occurrence of Fipronil in residential house dust in the presence and absence of pets: a hint for a comprehensive toxicological assessment. J. Environ. Sci. Health Part B 54 (6), 441–448. https://doi.org/10.1080/03601234.2019.1607133.

J. R. Thompson *et al.*, "Bacterial Diversity in House Dust: Characterization of a Core Indoor Microbiome," *Front. Environ. Sci.*, vol. 9. 2021, doi: 10.3389/fenvs.2021.754657.

J. R. Thompson *et al.*, "Bacterial Diversity in House Dust: Characterization of a Core Indoor Microbiome," *Front. Environ. Sci.*, vol. 9, 2021, Accessed: Mar. 01, 2024. [Online]. Available: https://www.frontiersin.org/articles/10.3389/fenvs.2021.754657.

Trinh, J., Schymanski, E.L., Smajic, S., Kasten, M., Sammler, E., Grünewald, A., 2022. Molecular mechanisms defining penetrance of LRRK2-associated Parkinson's disease. Med. Genet. 34 (2), 103–116. https://doi.org/10.1515/medgen-2022-2127.

Tsafaras, G., Baekelandt, V., 2022. The role of LRRK2 in the periphery: link with Parkinson's disease and inflammatory diseases. Neurobiol. Dis. 172, 105806. https://doi.org/10.1016/j.nbd.2022.105806.

H. Tsugawa *et al.*, "MS-DIAL: data-independent MS/MS deconvolution for comprehensive metabolome analysis," *Nat. Methods*, vol. 12, no. 6, Art. no. 6. 2015, doi: 10.1038/nmeth.3393.

T. Usnich *et al.*, "LIPAD (LRRK2/Luebeck International Parkinson's Disease) Study Protocol: Deep Phenotyping of an International Genetic Cohort," *Front. Neurol.*, vol. 12, 2021, Accessed: Dec. 08, 2023. [Online]. Available: https://www.frontiersin.org/articles/10.3389/fneur.2021.710572.

van der Merwe, D., Jordaan, A., van den Berg, M., 2019. "Case report: fipronil contamination of chickens in the Netherlands and surrounding countries", in *Chemical hazards in foods of animal origin*. Wageningen Academic 567–584. https://doi.org/10.3920/978-90-8686-877-3_23.

Varrette, S., Bouvry, P., Cartiaux, H., Georgatos, F., Jul. 2014. Management of an academic HPC cluster: The UL experience. In: 2014 International Conference on High Performance Computing & Simulation (HPCS), pp. 959–967. https://doi.org/10.1109/HPCSim.2014.6903792.

S. Vascellari *et al.*, "Gut Microbiota and Metabolome Alterations Associated with Parkinson's Disease," *mSystems*, vol. 5, no. 5, pp. e00561-20. 2020, doi: 10.1128/mSystems.00561-20.

von der Ohe, P., Aalizadeh, R., 2000. "S13 | EUCOSMETICS | Combined Inventory of Ingredients Employed in Cosmetic Products. And Revised Inventory (2006)". Zenodo 28, 2020. https://doi.org/10.5281/zenodo.3959386.

Westenberger, A., et al., 2024. Relevance of genetic testing in the gene-targeted trial era: the Rostock Parkinson's disease study. Brain 147 (8), 2652–2667. https://doi.org/10.1093/brain/awae188.

Xu, Y., et al., 2024. Effects and mechanisms of bisphenols exposure on neurodegenerative diseases risk: A systemic review. Sci. Total Environ. 919, 170670. https://doi.org/10.1016/j.scitotenv.2024.170670.

Yu, G., Xu, C., Zhang, D., Ju, F., Ni, Y., 2022. MetOrigin: Discriminating the origins of microbial metabolites for integrative analysis of the gut microbiome and metabolome. iMeta 1 (1), e10.